Article

Validation of COSMIC-2-Derived Ionospheric Peak Parameters Using Measurements of Ionosondes

Shuangshuang Shi [1,2], Wang Li [1,2], Kefei Zhang [1,2,3,*], Suqin Wu [1,2], Jiaqi Shi [1,2], Fucheng Song [4] and Peng Sun [1,2]

1   Jiangsu Key Laboratory of Resources and Environmental Information Engineering, China University of Mining and Technology, Xuzhou 221116, China; shshshi@whu.edu.cn (S.S.); liwang@cumt.edu.cn (W.L.); suqin_wu@cumt.edu.cn (S.W.); shijq@cumt.edu.cn (J.S.); sunpcxs@cumt.edu.cn (P.S.)
2   School of Environmental Science and Spatial Informatics, China University of Mining and Technology, Xuzhou 221116, China
3   Satellite Positioning for Atmosphere, Climate and Environment (SPACE) Research Centre, RMIT University, Melbourne, VIC 3001, Australia
4   Shandong Provincial Key Laboratory of Water and Soil Conservation and Environmental Protection, College of Resources and Environment, Linyi University, Linyi 276000, China; songfucheng@lyu.edu.cn
*   Correspondence: profkzhang@cumt.edu.cn

Abstract: Although numerous validations for the ionospheric peak parameters values (IPPVs) obtained from the Constellation Observing System for Meteorology, Ionosphere, and Climate (COSMIC) have been conducted using ionosonde measurements as a reference, comprehensive evaluations of the quality of the COSMIC-2 data are still undesirable, especially under geomagnetic storm conditions. In this study, the IPPVs measured by ionosondes (Ramey, Boa Vista, Sao Luis, Jicamarca, Cachoeira Paulista, and Santa Maria) during the period 1 October 2019 to 31 August 2021, are used to evaluate the quality of COSMIC-2 data over low-latitude regions of the Americas. The results show that the N_mF_2 (h_mF_2) from COSMIC-2 agrees well with the ionosonde measurements, and the correlation coefficients for the two sets of data at the above six stations are 0.93 (0.84), 0.91 (0.85), 0.91 (0.88), 0.88 (0.79), 0.96 (0.83), and 0.96 (0.87), respectively. The data quality of COSMIC-2 derived N_mF_2 is largely dependent on geomagnetic latitude. It was also found that N_mF_2 derived from COSMIC-2 tends to be underestimated over the stations in Boa Vista and Cachoeira Paulista, which are close to the crests of the equatorial ionization anomaly (EIA), whilst that of the other stations is slightly overestimated. A comparison between COSMIC-measured and ionosonde-derived h_mF_2 indicates that the former is systematically higher than the latter. In addition, the differences in the two N_mF_2 datasets derived from COSMIC-2 and ionosonde measurements at night are generally smaller than those of daytime, when the EIA is well developed, and vice versa for h_mF_2, whose RMSE is slightly smaller during daytime (with the exception of Ramey). Furthermore, N_mF_2 obtained from COSMIC-2 is shown to perform best in summer at Ramey, Boa Vista, Sao Luis, and Santa Maria, best in winter at Jicamarca and Cachoeira Paulista. Finally, the COSMIC-2 electron densities capture the ionospheric dynamic enhancements under a moderate geomagnetic storm condition very well.

Keywords: COSMIC-2; data validation; NmF2; hmF2; equatorial ionization anomaly; geomagnetic storm

1. Introduction

Global positioning system (GPS) radio occultation (RO) is a technique capable of sensing the atmosphere, due to its advantages of high vertical resolution, high precision, global coverage, and long-term stability [1–3]. The first-generation Constellation Observing System for Meteorology, Ionosphere, and Climate (COSMIC-1) constellation was launched into a circular low-earth orbit at the Vandenberg Air Force Base on 15 April 2006. It has been widely applied in many scientific research areas, such as meteorology, climate, ionosphere,

and gravity studies [4–7]. Given the success of COSMIC-1, a follow-up mission, COSMIC-2, was successfully launched into a low-inclination orbit by the United States and Taiwan, China on 25 June 2019. Compared with COSMIC-1, COSMIC-2 was expected to provide more atmospheric and ionospheric RO profiles over middle and low latitude regions.

Electron density profiles (EDPs) retrieved from COSMIC-1 have been widely used in ionospheric research, including in the studies of ionospheric phenomena [8–12], ionospheric physical structures [13,14], and the characteristics of ionospheric spatial-temporal variations [15,16]. EDPs can be retrieved from the total electron content (TEC) using the Abel inversion, based on several assumptions, particularly that of spherical symmetry [16,17]. Although the Abel inversion, under the premise of spherical symmetry, has a large number of errors in the equatorial areas [18] and E regions of the ionosphere [19,20], it is still applied to the retrieval process of COSMIC-2 EDPs, predominantly due to its simplicity. Over the past two decades, the peak density (N_mF_2) and peak height (h_mF_2) of the F2 layer obtained from COSMIC-1's EDPs had been validated by many researchers [15,16,20–27]. Results indicated that the COSMIC-1 ionospheric peak parameters values (IPPVs) agreed well with the observations from other ionospheric detection techniques and models, including ionosonde, incoherent scatter radar (ISR), and the International Reference Ionosphere (IRI) model [28,29].

It had been indicated in some literature that the EDPs derived from the COSMIC-1 constellation agreed well with those from ionosondes in Europe [16], Brazil [22], China [24,25], and southeast Asia [27]. The correlation coefficients between the IPPVs derived from the two techniques were dependent on local time, geomagnetic latitude, and the level of solar activity. The correlation coefficient was smallest in the near-equator region, particularly in the crests of the equatorial ionization anomaly (EIA) region. Furthermore, ISRs deployed in low- and mid-latitudes regions, including the Kharkov radar observatory (49.6° N, 36.3° E) [23], Millstone Hill (42.6° N, 71.5° W), and Jicamarca ISRs (11.9° S, 76.0° W) [20], were also used to evaluate the quality of COSMIC-1 data. The results revealed that the quality of the observations of ISRs was consistent with those from COSMIC-1, and the correlation between the measurements of space-borne and ground-based techniques was higher in mid-latitude regions. This is probably due to the horizontal gradient in mid-latitude regions being smaller than that of low-latitude regions. Larger horizontal gradients in low-latitude regions may cause larger errors in the retrieved electron density profiles. Finally, the COSMIC-1 profiles were also evaluated using the simulations of the IRI-2016 model, and the results showed that the GPS RO profiles agreed well with the vertical EDPs simulated by the IRI-2016 model [21].

Recently, the N_mF_2 and h_mF_2 values derived from COSMIC-2 RO during the period from 14 September 2019 to 16 October 2019 were compared with digisonde measurements over eight digisonde stations during daytime [30]. The results showed that the N_mF_2 and h_mF_2 from COSMIC-2 agreed with those from the digisonde data, and their correlation coefficients were both 0.885. Additionally, validation was also conducted during the geomagnetic storm period, and it was found that the correlation coefficients during the geomagnetic storm period were similar to those with the data span over the whole month. Cherniak et al. [31] validated foF_2 and h_mF_2 derived from COSMIC-2 RO during January–February 2020, using measurements from 29 ionosondes located globally at low and middle latitudes under quiet geomagnetic conditions. These two IPPVs were validated on a global scale, considering different longitudinal sectors (the American, Europe-African, and Asia-Pacific sectors), and different latitudinal zones (magnetic low and middle latitudes). Measurements obtained from ionosondes located in one sector or zone were put together for analysis, rather than detailed analysis of variations at each ionosonde. The conclusions described that the COSMIC-2 RO derived IPPVs showed good agreement with ionosonde measurements, and larger errors appeared in the IPPVs derived from the COSMIC-2 RO at low latitudes. Although the quality of COSMIC-2 data had been evaluated by some scholars using ionosonde measurements as referenced, few detailed validations of the IPPVs from COSMIC-2 RO over different latitudes in low-latitude re-

gions of the Americas have been conducted, not to mention the use of long-period data to investigate the characteristics of the IPPVs. This is the main reason for this research using approximately two years of sample data to study the spatial-temporal characteristics of COSMIC-2 ionospheric peak parameters values (i.e., COSMIC-2-IPPVs). In addition, due to the high ionospheric dynamics and the presence of large horizontal gradients that may introduce significant errors in the retrieval of EDPs over low latitude regions, validation of COSMIC-2 data over low latitude regions is very important from the point of view of understanding the mechanisms of ionospheric dynamics and practical applications.

In this study, ionosonde data at Ramey, Boa Vista, Sao Luis, Jicamarca, Cachoeira Paulista, and Santa Maria were used to validate the IPPVs obtained from COSMIC-2 measurements over low-latitude regions of the Americas. The diurnal, seasonal, and latitudinal variations in the N_mF_2 and h_mF_2 values from COSMIC-2 profiles were compared to those of the ionosondes. In addition, the response of COSMIC-2 observations to a moderate geomagnetic storm which occurred on 28 September 2020, was also investigated.

The outline of this paper is as follows: data selection and preprocessing for data matching between COSMIC-2 RO and ionosonde measurements are introduced in Section 2; the diurnal, seasonal, and latitudinal variation features of COSMIC-2-IPPVs under geomagnetic quiet conditions, as well as the latitudinal variation feature of COSMIC-2-IPPVs under geomagnetic storm conditions, are validated in Section 3. In addition, the responses of COSMIC-2-IPPVs to the moderate geomagnetic storm occurring on 28 September 2020, are also investigated in this section. Section 4 provides a brief discussion of the results. Conclusions are given in Section 5.

2. Datasets

The observations from the aforementioned ionosondes over low-latitude regions of the Americas were used to validate the quality of the IPPVs derived from the COSMIC-2 constellation under quiet and disturbed solar-geomagnetic conditions. Detailed information about the datasets is described in the following sections.

2.1. EDPs of COSMIC-2

The COSMIC-2 constellation, which includes six micro-satellites, was deployed into low-inclination orbits with an inclination of 24° at a 550 km altitude on 25 June 2019. The COSMIC-2's RO EDPs can be obtained from the COSMIC Data Analysis and Archive Centre (CDAAC) via the website https://www.cosmic.ucar.edu/ (accessed on 2 September 2021). Currently, approximately 4000 EDPs can be collected by the COSMIC-2 constellation daily, and these profiles play an important role in exploring ionospheric dynamic evolution over low and middle latitudes. The spatial distribution of the daily COSMIC-2 EDPs on 10 August 2020, is shown in Figure 1a, and the numbers of the daily COSMIC-2 EDPs during the approximately 2 year period from 1 October 2019 to 31 August 2021, are shown in Figure 1b. It can be seen that all of the EDPs are at latitudes within 40° S–40° N, and the number of the daily EDPs demonstrated an increasing trend, roughly, with some small fluctuations. The number of occultation increases by day in Figure 1b is that the main payload instrument of the COSMIC-2 mission, the Tri-GNSS Radio-Occultation Receiver System (TGRS), becomes more stable than it was in the beginning, and the payload can operate normally for a longer period of time.

In the data pre-processing stage, the quality of the COSMIC-2 RO EDPs was checked. To reduce the errors caused by a large-scale spatial span, only the EDPs that had a latitude span under 10° and a longitude span under 15° were selected [32,33]. Moreover, the peak height of the F2 layer usually occurs above 200 km and under 500 km altitudes; thus, in this study, the EDPs that had peak heights beyond the range 200–500 km were removed. Furthermore, the Chapman α function was used to simulate the EDPs, and the correlation coefficients between the EDPs from COSMIC-2 RO and the simulations were computed. The results indicated that the EDP fluctuated largely when the correlation coefficients were

under 0.9. Therefore, the EDPs whose correlation coefficients were under 0.9 were also removed.
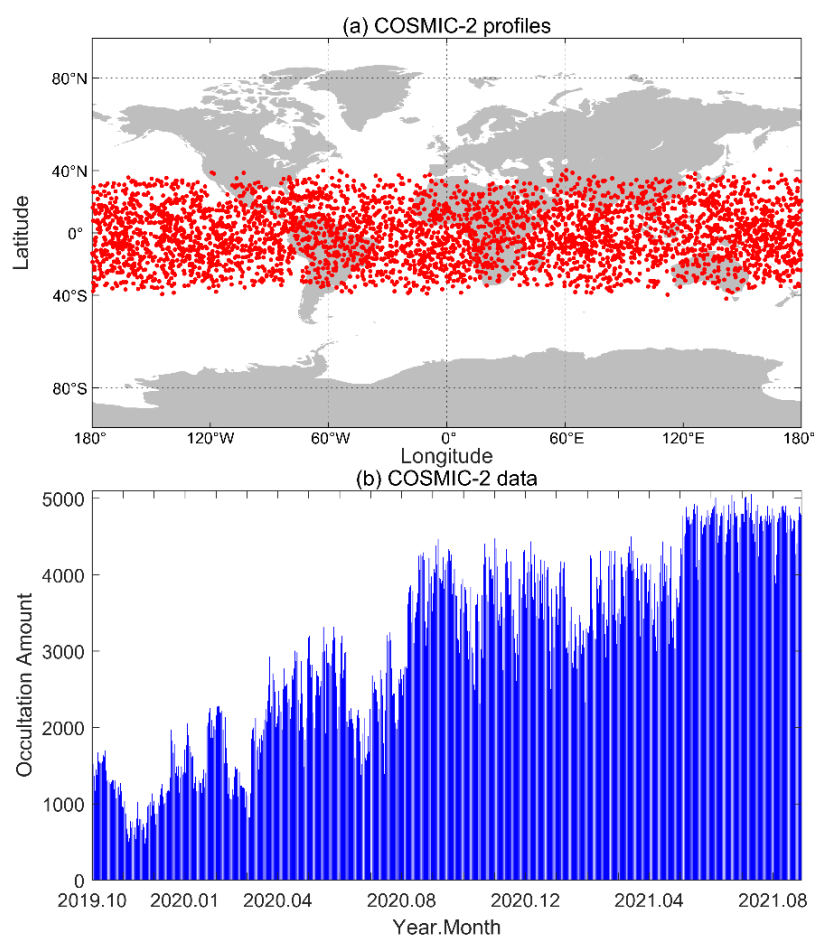

Figure 1. (**a**) Spatial distribution of daily COSMIC-2 RO EDPs on 10 August 2020, where each red point denotes the location of the peak density for each EDP; and (**b**) the numbers of daily COSMIC-2 RO EDPs in the approximately 2-year period from October 2019 to August 2021.

2.2. Indices of Solar Activity

The solar radio flux at 10.7 cm (F10.7 index) downloaded from the Goddard Space Flight Center (https://omniweb.gsfc.nasa.gov/, accessed on 2 September 2021) was used to represent solar activity. The red line in Figure 2a shows the daily variation of the F10.7 index during the approximately 2-year period from 1 October 2019, to 31 August 2021, during which time solar activity was quiet. The annual mean F10.7 index, which was based on data of the approximately 2-year period, was under 75.

2.3. Indices of Geomagnetic Activity

The intensity of global geomagnetic activity can be denoted by the ap index, which can be obtained from the Helmholtz Centre Potsdam–GFZ German Research Centre for Geosciences (https://www.gfz-potsdam.de/, accessed on 2 September 2021). The green line in Figure 2b shows the temporal variation of the 3-h ap index. In this study, the COSMIC-2 EDPs were divided into two groups according to the value of 3-h ap index: one group was for analysis under quiet geomagnetic conditions (ap < 15), and the other was for analysis under geomagnetic storm conditions (ap $\geq$ 15).
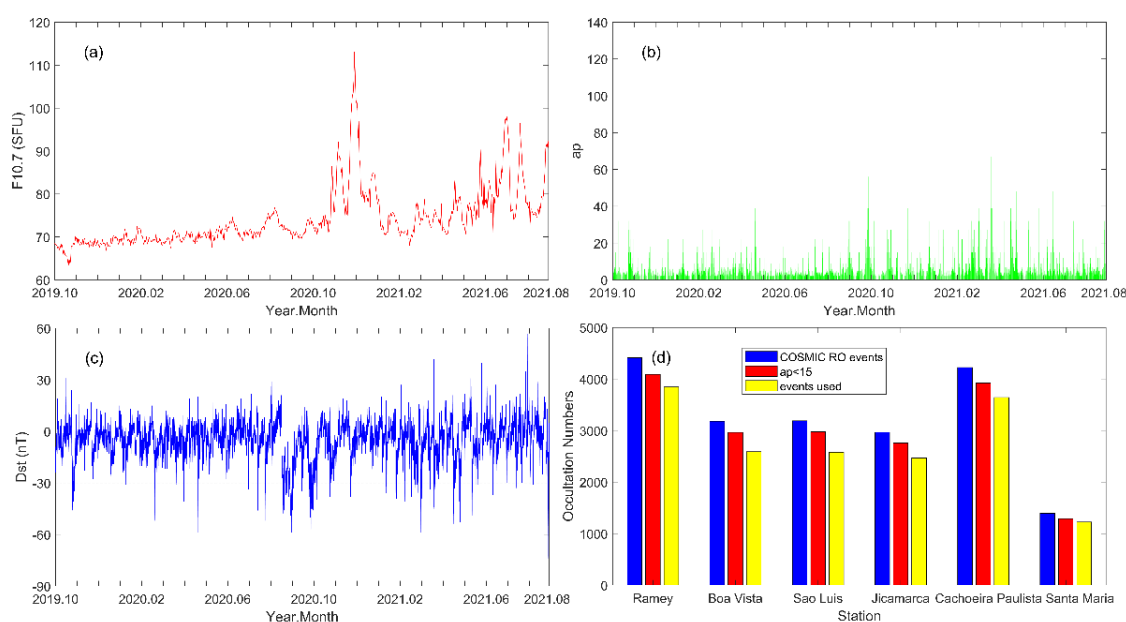
Figure 2. Daily solar-geomagnetic activities in the approximately 2-year period from 1 October 2019, to 31 August 2021. (**a**) F10.7; (**b**) ap; (**c**) Dst; (**d**) total number of COSMIC-2 EDPs over each ionosonde station.

Since the validation of the IPPVs retrieved from COSMIC-2 EDPs was also conducted under geomagnetic storm conditions, the Dst index obtained from the World Data Center for Geomagnetism, Kyoto (http://wdc.kugi.kyoto-u.ac.jp/, accessed on 2 September 2021), was used to determine the intensity of a geomagnetic storm. The Dst time series in Figure 2c show that several minor-to-moderate geomagnetic storms occurred during the study period, with Dst values between −60 and −30 nT [34]. A moderate geomagnetic storm occurred on 28 September 2020. In this study, the COSMIC-2 EDPs on 27–28 September 2020, were selected to investigate the variation under a disturbed geomagnetic condition.

2.4. Ionosonde Data

Since ionosonde is ground-based ionospheric detection equipment, and can directly measure the ionosphere, it has been used as a reference for COSMIC RO observations. To validate the COSMIC-2-IPPVs, the critical frequency ($foF2$) and peak height (h_mF_2) of the F2 layer provided by the Global Ionosphere Radio Observatory (GIRO) with Real-Time & Retrospective HF Ionospheric Sounding Data from the Lowell DIDBase (http://giro.uml.edu/didbase/scaled.php, accessed on 2 September 2021) were used as raw dataset in this study. The SAO Explorer application connected to the GIRO databases was used to check all auto-scaled ionogram traces. If the auto-scaled ionogram trace was incorrect, the ionogram was manually scaled using the SAO Explorer application in order to obtain the true peak parameter values. The IPPVs derived from the six ionosondes over low-latitude regions of the Americas were used as the reference points of the validation. Detailed information about the six ionosonde stations (Ramey, Boa Vista, Sao Luis, Jicamarca, Cachoeira Paulista, and Santa Maria) are presented in Table 1, and locations of all ionosondes in low-latitude regions of the Americas are shown in Figure 3. It can be seen from Figure 3 that there are nine ionosondes available in this region, and the six ionosondes marked with red pentagrams distributed in different latitudes and distanced from each other were used in this study. Sao Luis and Jicamarca are close to the geomagnetic equator, and Boa Vista and Cachoeira Paulista are close to the EIA crest. The total number of COSMIC-2 RO profiles over each of the six stations in the approximately 2-year period from 1 October 2019 to 31 August 2021 is shown in Figure 2d, where the blue bar denotes the total number of RO events; the red bar denotes the total number of RO events under quiet geomagnetic

conditions (3-h ap < 15); and the yellow bar denotes the total number of RO events after quality control was performed.

Table 1. Geographic and geomagnetic locations of the six ionosonde stations used.

Station	Geographic Longitude (° E)	Geographic Latitude (° N)	Geomagnetic Latitude (° N)
Ramey	−67.10	18.50	27.75
Boa Vista	−60.70	2.80	11.98
Sao Luis	−44.20	−2.60	5.69
Jicamarca	−76.80	−12.00	−2.54
Cachoeira Paulista	−45.00	−22.70	−14.17
Santa Maria	−53.71	−29.73	−20.63
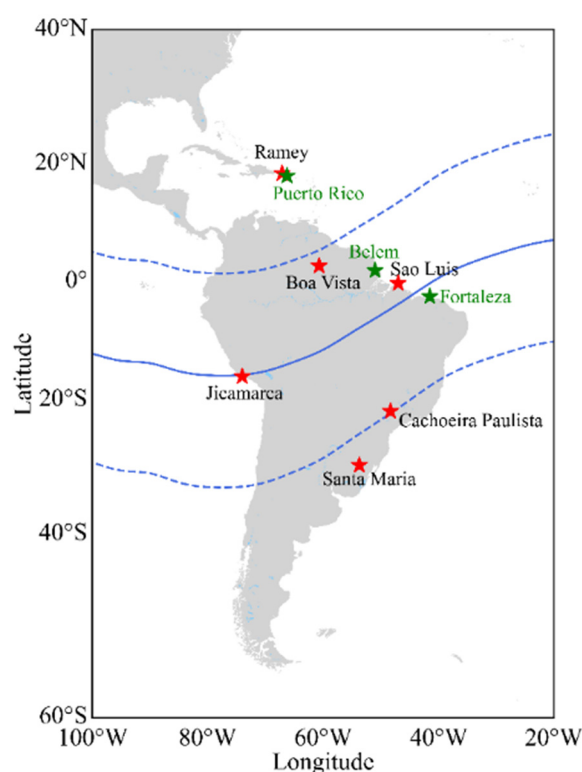
Figure 3. Schematic for locations of the ionosondes available over low-latitude regions of the Americas. Ionosondes marked with red pentagrams were used in this study. Lines show the magnetic equator and ±15° of the magnetic latitude.

Two steps for the selection of sample profiles are as follows: in the first step, if the tangent point of the peak density for the COSMIC-2 RO profile occurred near the given ionosonde station (with a maximum latitude difference of 3° and a maximum longitude difference of 5°), then the profile was selected. In the second step, if the time difference between the selected COSMIC-2 RO observation and ionosonde data was under 7.5 min, the data pair was selected. The total numbers of finally selected data pairs for Ramey, Boa Vista, Sao Luis, Jicamarca, Cachoeira Paulista, and Santa Maria during the approximately 2-year period studied were 2227, 1159, 1437, 998, 1723, and 658, respectively.

### 3. Results

3.1. Latitudinal Dependence

Since COSMIC RO observations vary with latitude, many researchers have analyzed the latitudinal difference in COSMIC performances [25,27,35]. In this study, the latitudinal variation of COSMIC-2-IPPVs under both quiet and disturbed geomagnetic conditions was investigated, and the statistical results are shown in Figure 4a–l (the first two columns) are

the scatter plots of N_mF_2 (the green dots) and h_mF_2 (the red dots) values obtained from COSMIC-2 and ionosonde over each station under quiet geomagnetic conditions in the approximately 2-year period studied. Figure 4m–x (the third and fourth columns) are the results found during a geomagnetic storm period with a 3-h ap index exceeding 15. In each of the subfigures, the abscissa axis and vertical axis represent the COSMIC-2 and ionosonde results, respectively; the black line shows the trend of the fitting function; R is the correlation coefficient; and N is the number of the data pairs in the samples. The correlation coefficients in the first column are significantly larger than those of the second column in the same row; and the R values at Ramey, Boa Vista, Sao Luis, Jicamarca, Cachoeira Paulista, and Santa Maria range from 0.88 to 0.96, indicating good agreements between N_mF_2 from COSMIC-2 EDPs and the ionosonde measurements at these stations. The Jicamarca station is located close to the geomagnetic equator (an EIA valley), where the electron density is much smaller than in the EIA crests region. The two N_mF_2 datasets obtained from COSMIC-2 EDPs and the ionosonde measurements have the lowest correlation (0.88) at Jicamarca, which is likely due to the neglect of the larger horizontal gradients in the retrieval of the electron density profiles at this station [15,20,27,36]. The slopes of 0.91, 1.01, 0.89, 0.80, 1.02, and 0.94 for the N_mF_2 fitting lines over the six stations also indicate good agreements, since these values are close to 1. Furthermore, the N_mF_2 values from COSMIC-2 at Ramey, Sao Luis, Jicamarca, and Santa Maria tend to be overestimated, especially over Jicamarca. At Boa Vista and Cachoeira Paulista, COSMIC-2 N_mF_2 tends to be underestimated, as their slopes are larger than 1. The second column shows that the R values of h_mF_2 at Ramey, Boa Vista, Sao Luis, Cachoeira Paulista, and Santa Maria are 0.84, 0.85, 0.88, 0.83, and 0.87, respectively, which indicates a good agreement between the COSMIC-retrieved h_mF_2 and ionosonde observations. The h_mF_2 result at Jicamarca has the lowest correlation (0.79), and one of the possible reasons is that the latitudinal gradient in electron density over this station is higher than over the other five stations; consequently, the assumption of spherical symmetry for the inversion algorithm is violated [22]. The slopes in the second column indicate that h_mF_2 obtained from COSMIC-2 tends to be overestimated at each of the six stations. This suggests that h_mF_2 calculated from manually scaled ionograms using the SAO Explorer software [37–39] seems to be systematically underestimated, thus, the inversion technique used for the ionosonde h_mF_2 needs to be investigated in detail [40]. Good agreement between IPPVs derived from COSMIC-2 RO and ground-based ionosonde measurements can also be found in the studies of Lin et al. [30] and Cherniak et al. [31]. Lin et al. [30] found that IPPVs derived from eight selected digisonde stations located at low- and mid-latitudes agree well with those from COSMIC-2 during daytime periods from 14 September to 16 October 2019, and the correlation coefficients between them were 0.885 (N_mF_2) and 0.885 (h_mF_2). In the study of Cherniak et al. [31], comparison results for foF_2 and h_mF_2 derived from COSMIC-2 RO against ionosonde data revealed a high degree of correlation on a global scale, and in the American, Europe–African, and Asia–Pacific sectors.

The third column panels (m)–(r), which represent the scatter plots of N_mF_2 under geomagnetic storm conditions, all show large R values: 0.96, 0.91, 0.95, 0.91, 0.95, and 0.99, which is different from the above case (during a quiet geomagnetic period), in that the R value at Jicamarca is much smaller than at the other five stations. Furthermore, the R values are slightly larger than those of the first column at the same station. These results are consistent with the findings by Lin et al. [30], who found that the correlation coefficients between N_mF_2 obtained from COSMIC-2 and digisondes during a period studied and a geomagnetic storm period were 0.885 and 0.898, respectively. Compared with the second column, the last column panels (s)–(x) show that the h_mF_2 values obtained from COSMIC-2 and ionosonde also have good agreement during the geomagnetic storm period, with increased correlation coefficients (except for Boa Vista and Cachoeira Paulista). The above results illustrate that the correlation coefficients during the storm period are generally similar to or greater than those of a quiet geomagnetic period. However, longer observation

times with more sample data are requried for the validation of COSMIC-2-IPPVs during geomagnetic storm periods.
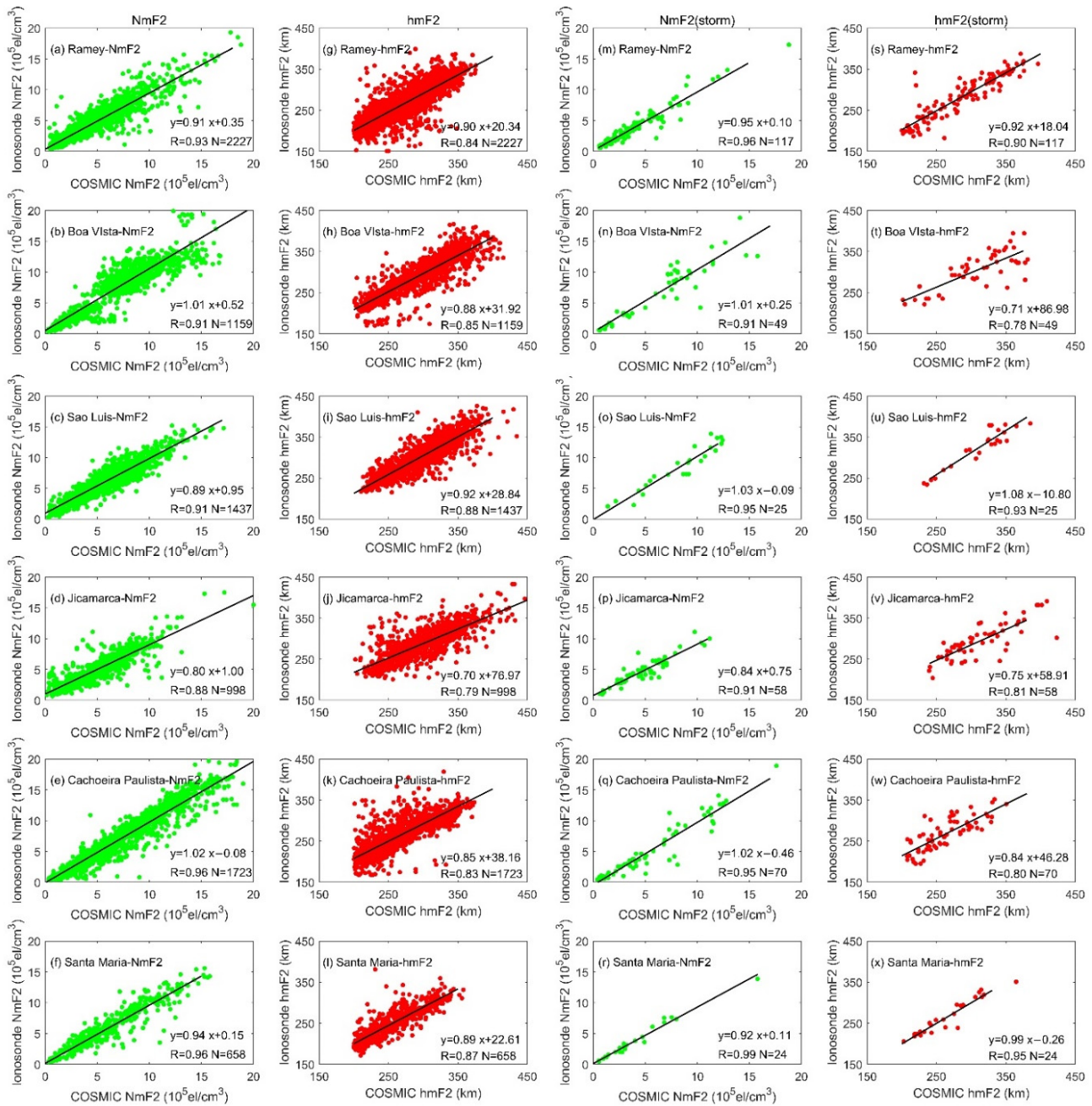
Figure 4. Scatter plots of N_mF_2 (green dots) and h_mF_2 (red dots) obtained from COSMIC-2 observations and ionosonde measurements at each station. The black lines are the trends of fitting functions; R is the correlation coefficient; and N is the number of data pairs. The first two columns (**a**–**l**) and the last two columns (**m**–**x**) are for quiet and geomagnetic storm conditions, respectively.

For a further analysis of errors for the COSMIC-2-IPPVs, the absolute error (denoted by Abs$_E$) and relative error (denoted by Rel$_E$), defined below, were used in this study:

$$Abs_E = COSMIC - Ionosonde \qquad (1)$$

$$Rel_E = (COSMIC - Ionosonde)/Ionosonde \times 100\% \qquad (2)$$

where COSMIC and Ionosonde represent the COSMIC-2-IPPVs and ionosonde ionospheric peak parameter values (ionosonde-IPPVs), respectively.

Figure 5 shows the histograms of the absolute (red) and relative (green) errors of N_mF_2 (first two columns) and h_mF_2 (last two columns) at each of the six stations. The first column shows that, with the exceptions of Boa Vista and Cachoeira Paulista (the second and fifth rows), the absolute errors of N_mF_2 at Ramey, Sao Luis, Jicamarca, and Santa Maria all follow a normal distribution, with most values ranging from -0.3×10^6 to 0.3×10^6 el/cm^3; and their RMSEs are 1.00×10^5 el/cm^3, 1.10×10^5 el/cm^3, 1.26×10^5 el/cm^3, and 0.99×10^5 el/cm^3, respectively. At Boa Vista and Cachoeira Paulista, most absolute errors are negative, demonstrating an underestimation of N_mF_2 from COSMIC-2 at these two stations, and their RMSEs are 1.76×10^5 el/cm^3 and 1.35×10^5 el/cm^3. Similar results can also be seen from the second column: the mean relative errors of N_mF_2 at Boa Vista and Cachoeira Paulista are negative, whilst the results at the other four stations are positive.

The third column panels (m)–(r) are the histograms of the absolute errors of h_mF_2, which show that most of the absolute errors of h_mF_2 are larger than 0 at all the six stations, meaning an overestimation of the COSMIC-2 results, and the corresponding RMSEs are 25.62 km, 25.62 km, 21.32 km, 30.37 km, 23.82 km, and 20.06 km, respectively. Similar results are also shown in the fourth column: the mean relative errors of h_mF_2 at the six stations are positive, with the corresponding mean relative errors of 3.13%, 1.82%, 1.46%, 4.21%, 0.98%, and 2.69%, respectively.

It can be seen from the above results that N_mF_2 values derived from COSMIC-2 varied with geomagnetic latitude; they tended to be overestimated at the stations near the geomagnetic equator (Jicamarca and Sao Luis) and at higher geomagnetic latitudes (Ramey and Santa Maria), whilst the stations close to the EIA crests (Boa Vista and Cachoeira Paulista) tended to be underestimated, which is probably caused by the EIA. The EIA is the most significant feature of the ionosphere in low-latitude areas, characterized by the fact that electron density in the low-latitude geomagnetic belt is not evenly distributed during daytime; there is a depletion along the geomagnetic equator and an enhancement in the off-equator region (center at ±10–15°, geomagnetic). The phenomenon is led by vertically upward ionospheric drift movements, caused by a horizontal magnetic field near the geomagnetic equator, and an imposed eastward electric field during daytime [15]. Thus, when the COSMIC-2 RO EDPs are retrieved by the Abel inversion under the assumption of spherical symmetry, the TEC horizontal gradient along GPS rays caused by the EIA may introduce errors in the EDPs. As a result, the high electron density over Boa Vista and Cachoeira Paulista, which are near the EIA crests, will be averaged to the whole ray path in the inversion process. This will lead to an underestimation of the N_mF_2 obtained from COSMIC-2 at these stations (in comparison with the reference result from ionosonde observations). In contrast, the electron density at the other four ionosondes is much smaller; hence, when the GPS signal transits through the EIA crests, the electron density along the propagation path increases significantly, resulting in increased electron density over the four ionosondes. Therefore, N_mF_2 retrieved from COSMIC-2 at these stations is overestimated. Similar results have also been stated in several studies [18,20,25,27,35]. In particular, Liu et al. [15] examined the IPPVs obtained from COSMIC-1 and the ground-based digisonde portable sounder DPS-4 at Jicamarca in 2007, which showed that the N_mF_2 at Jicamarca was being overestimated by the Abel inversion on the enhanced TEC when the EIA pronouncedly appeared.
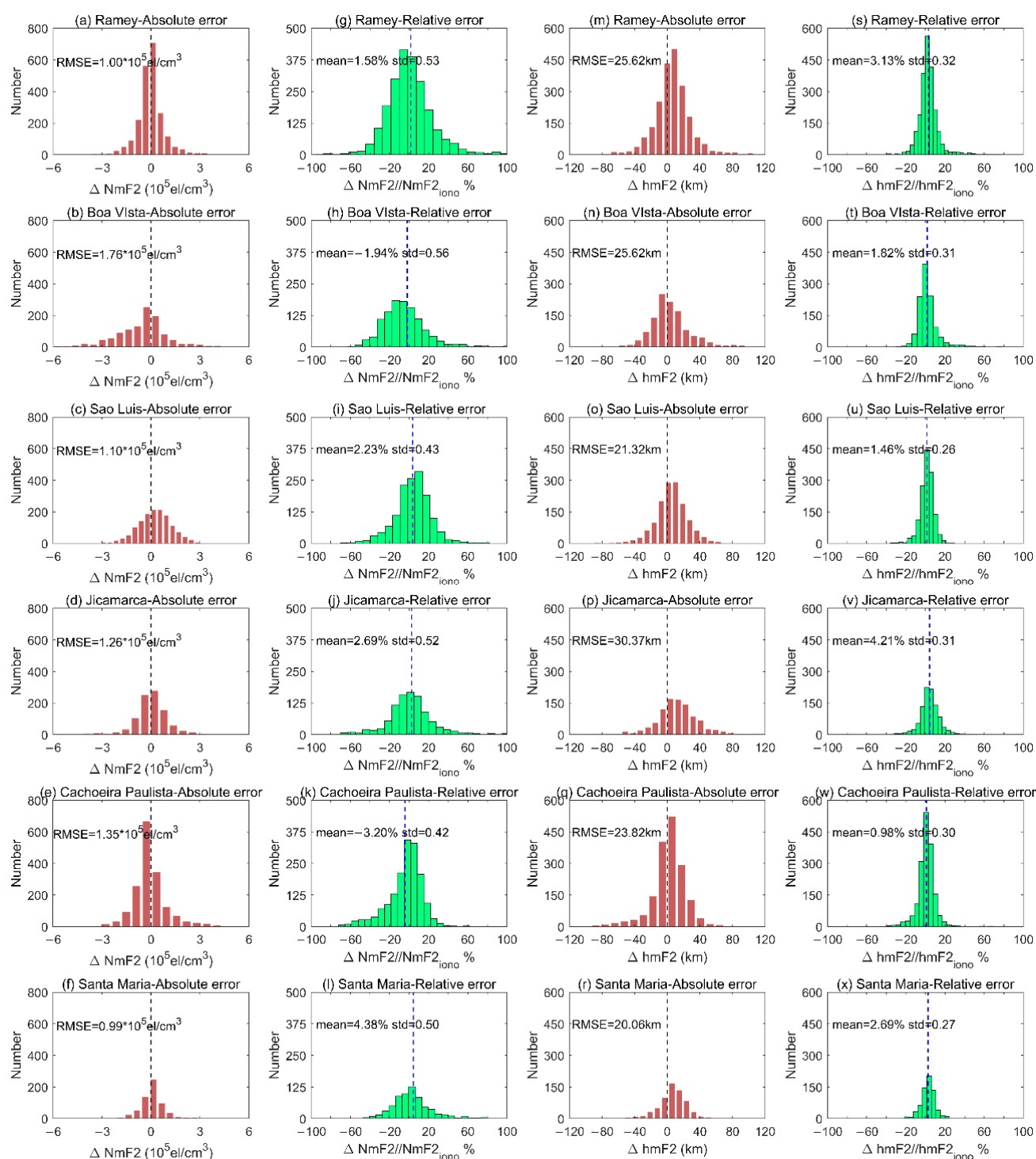
Figure 5. Histograms of the absolute (in red) and relative (in green) errors of N_mF_2 (**first two columns**) and h_mF_2 (**the last two columns**) at each station. The black lines in the first and third columns represent (x = 0), and the blue lines in the second and fourth columns represent (x = mean).

Moreover, it can be drawn from the comparison between errors of N_mF_2 (the first two columns in Figure 5) and h_mF_2 (the last two columns in Figure 5) that there is a discrepancy in their latitudinal variation. The RMSE of N_mF_2 is smaller at higher geomagnetic latitudes (Ramey and Santa Maria), whilst being more significant at the stations close to the geomagnetic equator (Jicamarca and Sao Luis), and most significant at the station located close to the northern EIA crest (Boa Vista). This is consistent with the findings of Hu et al. [25], who found that at higher latitude stations, the differences between COSMIC N_mF_2 and those

of ionosondes are very slight. The variation in the RMSE of h_mF_2 is irregular; the most significant RMSE value occurs at Jicamarca, and the RMSE at Cachoeira Paulista is smaller than that of Boa Vista. The distribution of the relative error of h_mF_2 is more concentrated around 0 than that of N_mF_2, and their distribution ranges are within -20 to 20% and -40 to 40%, respectively. Some statistical values for the above mentioned six ionosondes are shown in Table 2. The mean $|Rel_E|$ and mean absolute error (MAE) of N_mF_2 and h_mF_2 are also provided. The mean $|Rel_E|$ is averaged from the absolute value of relative errors in order to avoid the neutralization effect caused by the sign of relative errors. The mean $|Rel_E|$ of N_mF_2 at the six stations are 17.86%, 20.01%, 18.99%, 19.26%, 19.64%, and 16.00%, and that of h_mF_2 at the six stations are 7.06%, 6.46%, 5.25%, 7.95%, 6.08%, and 5.99%. The mean $|Rel_E|$ of N_mF_2 has a significant geomagnetic latitude dependency, and the mean $|Rel_E|$ of h_mF_2 is much smaller than that of N_mF_2 at each station.

Table 2. Statistics of the differences in N_mF_2 and h_mF_2 obtained from the COSMIC-2 and ionosonde (as the reference) at the six ionosondes under quiet geomagnetic conditions.

Station	N_mF_2				h_mF_2			
	R	RMSE (10^5 el/cm^3)	MAE (10^5 el/cm^3)	Mean $|Rel_E|$ (%)	R	RMSE (km)	MAE (km)	Mean $|RelE|$ (%)
Ramey	0.93	1.00	0.62	17.86	0.84	25.62	17.80	7.06
Boa Vista	0.91	1.76	1.25	20.01	0.85	25.62	18.11	6.46
Sao Luis	0.91	1.10	0.86	18.99	0.88	21.32	15.90	5.25
Jicamarca	0.88	1.26	0.82	19.26	0.79	30.37	22.60	7.95
Cachoeira Paulista	0.96	1.35	0.90	19.64	0.83	23.82	15.81	6.08
Santa Maria	0.96	0.99	0.61	16.00	0.87	20.06	14.90	5.99

3.2. Diurnal Variation Result

To investigate the performances of N_mF_2 and h_mF_2 in different hours, the hourly means of N_mF_2 and h_mF_2 from COSMIC-2 RO EDPs and the ionosonde measurements during the approximately 2-year period studied, and the hourly RMSEs based on all the data within the hour were calculated for each station. The results of N_mF_2 and h_mF_2 are shown in the left and right columns, respectively, in Figure 6. The first row (at Ramey) shows an overestimation of COSMIC-2 N_mF_2 (left) during the period from 8:00LT to 20:00LT, whilst the second row (at Boa Vista) shows a noticeable underestimation of COSMIC-2 N_mF_2 (left) during the period from 10:00LT to 20:00LT, and a slight overestimation during the period from 7:00LT to 9:00LT. Similarly, the third row (at Sao Luis) describes an underestimation of COSMIC-2 N_mF_2 during the periods from 6:00LT to 12:00LT and 21:00LT to 23:00LT; the fourth row (at Jicamarca) indicates an overestimation of COSMIC-2 N_mF_2 during the period from 13:00LT to 19:00LT, and an underestimation during the period from 21:00LT to 03:00LT; the fifth row (at Cachoeira Paulista) shows an overestimation of COSMIC-2 N_mF_2 during the period from 17:00LT to 23:00LT; the last row (at Santa Maria) shows an overestimation of COSMIC-2 N_mF_2 during the period from 16:00LT to 22:00LT. Furthermore, the left column shows that the minimum daily N_mF_2 values at all of the six stations fall into the period from 4:00LT to 5:00LT, while the peak daily N_mF_2 values occur at different times: 15:00LT (at Ramey), 16:00LT (at Sao Luis), 15:00LT (at Jicamarca), and 14:00LT (at Santa Maria). In addition, two peaks can be observed at Boa Vista (second row) at 14:00LT and 16:00LT, and Cachoeira Paulista (fifth row) at 16:00LT and 18:00LT. For statistical analyses, the 10:00–18:00LT and 19:00–09:00LT periods were selected to represent daytime and nighttime, respectively. The RMSE of N_mF_2 during the daytime period at the six stations are 1.26×10^5 el/cm^3, 2.02×10^5 el/cm^3, 1.28×10^5 el/cm^3, 1.30×10^5 el/cm^3, 1.33×10^5 el/cm^3, and 1.30×10^5 el/cm^3, and those of nighttime are 0.83×10^5 el/cm^3, 1.36×10^5 el/cm^3, 1.05×10^5 el/cm^3, 0.84×10^5 el/cm^3, 1.28×10^5 el/cm^3, and 0.46×10^5 el/cm^3, which demonstrates that the RMSE of N_mF_2 during nighttime is smaller than during daytime at all of the six stations. This is consistent with the results of the validation for COSMIC-1 IPPVs by the measurements of an ionosonde

chain in China, that the RMSE of N_mF_2 is higher during the daytime than during the nighttime at each of the four stations [25]. At Boa Vista, the RMSE of N_mF_2 is the largest during both daytime and nighttime. The corresponding mean $|\text{Rel}_E|$ of N_mF_2 during the daytime period are 14.61%, 15.98%, 13.27%, 14.07%, 15.64%, and 14.74%, and those of nighttime are 19.41%, 25.26%, 19.61%, 21.20%, 24.15%, and 14.33%, respectively.
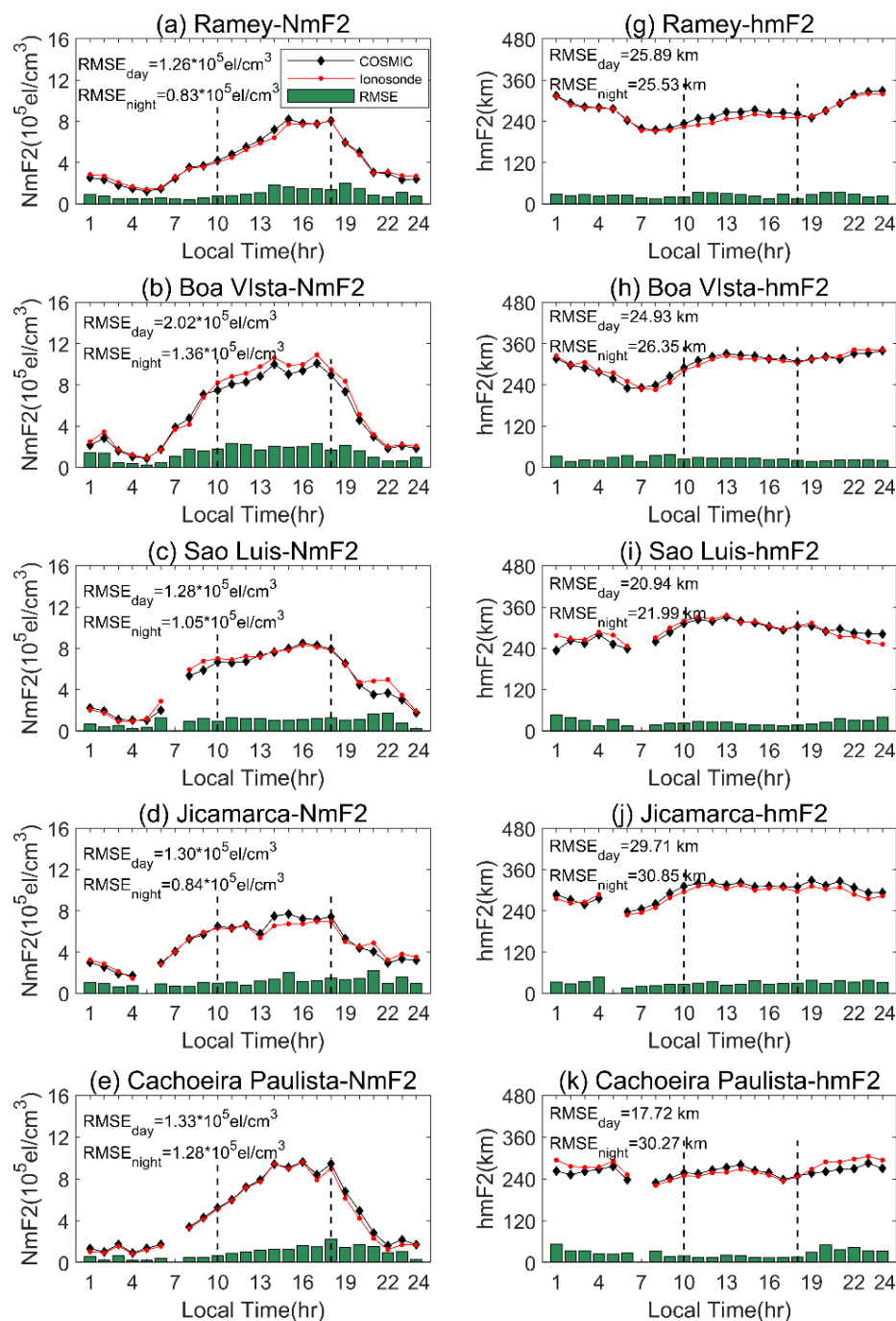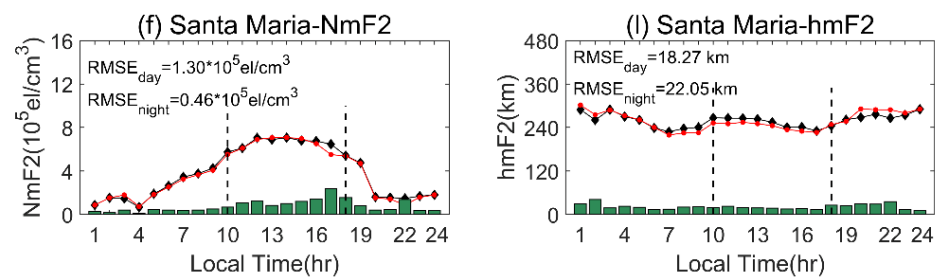

Figure 6. *Cont.*
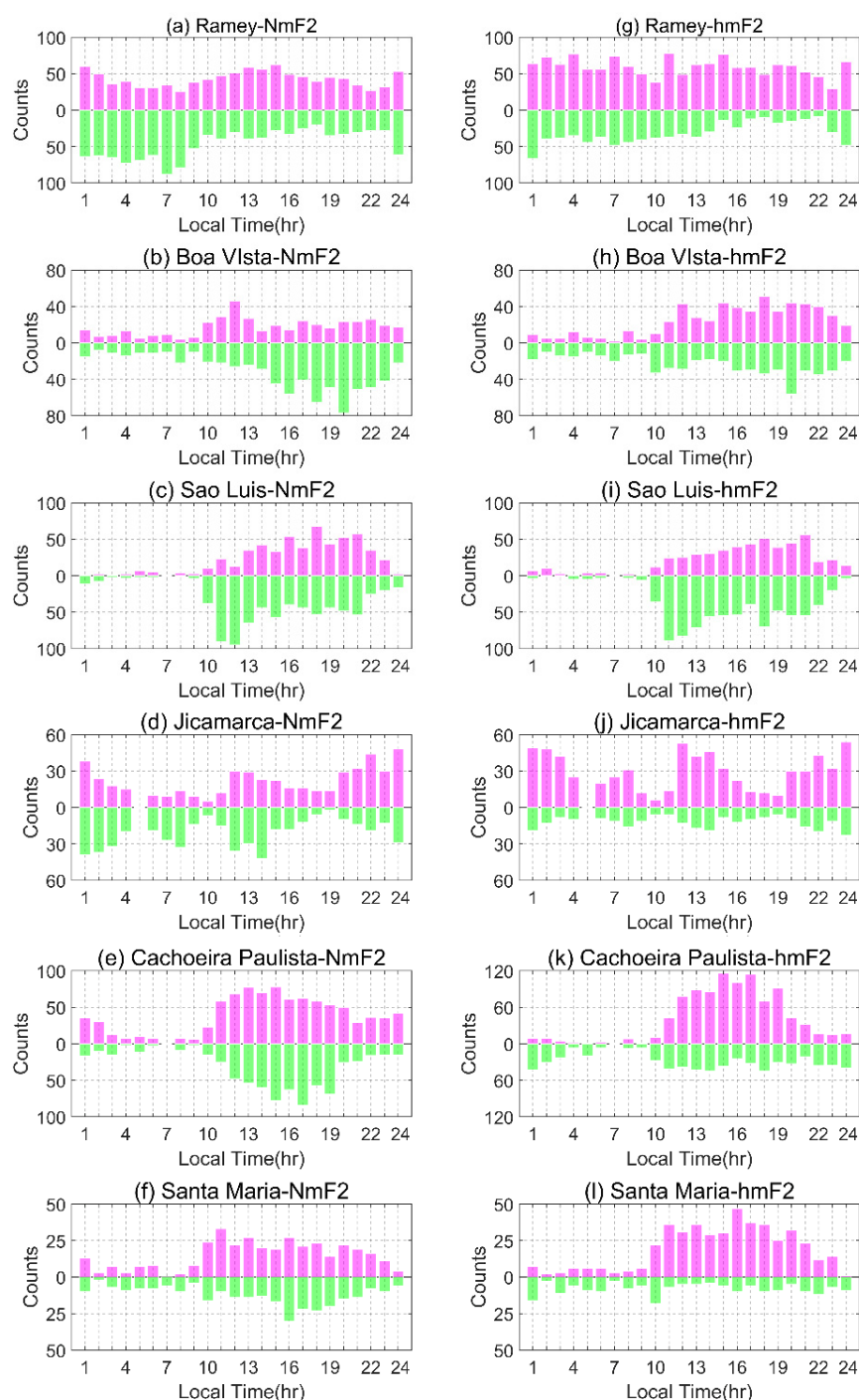
Figure 6. Hourly mean of N_mF_2 (**left column**) and h_mF_2 (**right column**) of the COSMIC-2-IPPVs (black squares) and ionosonde-IPPVs (red squares), respectively, during the approximately 2-year period studied at each station, and hourly RMSEs (green bars). The two vertical dashed lines in each subfigure denote the start and end moments of the daytime.

The right column panels (g)–(l) all show a good agreement of h_mF_2 resulting from COSMIC-2 observations and ionosonde measurements. The h_mF_2 values obtained from COSMIC-2 tend to be slightly overestimated during the daytime, and underestimated during some local times in the night at Boa Vista, Sao Luis, Cachoeira Paulista, and Santa Maria, which is different from the results obtained by Chu et al. [40]. They found that, irrespective of local time, the COSMIC-1 average peak heights are systematically higher than the average values of h_mF_2 from ionosondes by approximately 3–20%. The RMSEs of h_mF_2 at the six stations are 25.89 km, 24.93 km, 20.94 km, 29.71 km, 17.72 km, and 18.27 km during daytime, and 25.53 km, 26.35 km, 21.99 km, 30.85 km, 30.27 km, and 22.05 km during nighttime. With the exception of Ramey, the RMSE of h_mF_2 at other ionosondes during daytime is smaller than during nighttime. The corresponding mean $|\text{Rel}_E|$ of h_mF_2 during the daytime period are 7.82%, 6.08%, 4.88%, 7.52%, 5.18%, and 5.91%, and those of nighttime are 6.72%, 6.92%, 5.79%, 8.20%, 7.30%, and 6.11%. Detailed statistics of the hourly RMSE and hourly mean $|\text{Rel}_E|$ for N_mF_2 and h_mF_2 can be seen in Tables A1 and A2 in Appendix A.

For bias analyses, Figure 7 shows the numbers of the positive (in magenta) and negative (in green) difference values of the N_mF_2 (left column) and h_mF_2 (right column) resulting from COSMIC-2 and the ionosonde during each hour. From the left column, the top panel (at Ramey) reveals an overestimation of COSMIC-2 N_mF_2 during the 10:00–21:00LT period, and an underestimation in the other hours; the second panel (at Boa Vista) shows an overestimation in the 10:00–13:00LT period; the third panel (at Sao Luis) reveals an overestimation at 16:00LT, and during the 18:00–23:00LT period; the fourth panel (at Jicamarca) indicates an underestimation during the 01:00–14:00LT period, and an overestimation during the 15:00–24:00LT period; the fifth panel (at Cachoeira Paulista) shows an underestimation during the 15:00–19:00LT period; the bottom panel (at Santa Maria) shows an overestimation at 1:00LT, and during the 09:00–15:00LT and the 20:00–23:00LT periods. The right column shows that most occultation events (except those over Sao Luis) tend to overestimate h_mF_2. The prevailing numbers of positive/negative variations for each hour shown in Figure 7 which do not correspond to the sign of the hourly means shown in Figure 6 may be due to different analytical perspectives used. For instance, even if the prevailing underestimation at 14:00LT is shown in Figure 7d, the bigger values of positive variation may lead to the hourly mean of N_mF_2 from COSMIC-2, larger than that from ionosonde as shown in Figure 6d.

Figure 7. Numbers of the positive (magenta) and negative (green) difference values of N_mF_2 (**left column**) and h_mF_2 (**right column**) resulting from COSMIC-2 and ionosonde at each station for bias analyses.

3.3. Seasonal Variation Result

The hourly mean results presented in the above sections are based on the approximately 2-year data in each hour, which can be called an hourly mean. In this section, the statistical RMSE results are from three periods of time: summer, winter, and equinox, which are shown in Figure 8 for the comparisons of seasonal results. Due to the fact that the same time in the two hemispheres is opposite in terms of season, the three seasons are defined as follows. For the Ramey and Boa Vista stations, which are located in the northern hemisphere, the periods from May to August and November to February were defined

as summer and winter, respectively. In contrast, due to the other four stations, Sao Luis, Jicamarca, Cachoeira Paulista and Santa Maria, being located in the southern hemisphere, the above two periods were defined inversely as winter and summer, respectively. The rest two periods, i.e., from March to April, and from September to October, were defined as the equinox periods for all six stations. From the RMSE results shown in Figure 8a, it can be seen that, at Boa Vista, the RMSEs of N_mF_2 during equinox and winter are significantly larger than those of the other stations, and among the three seasonal results, the minimum and maximum occur in summer (red) and winter (yellow), respectively; at Ramey, Sao Luis, and Santa Maria, similar but much smaller RMSE values than those of Boa Vista are observed. However, at both Jicamarca and Cachoeira Paulista, the RMSE in winter (yellow) is smaller than in summer (red). This phenomenon may be caused by the asymmetry of the EIA and larger electron density for the southern EIA crest in summer than in winter, which causes a larger electron density gradient in summer at the Jicamarca and Cachoeira Paulista stations. However, in the research of Chuo et al. [41], comparison of the characteristics of IPPVs obtained from COSMIC-1 and digisonde over Ascension Island (8.0° S, 14.4° W, geomagnetic latitude 2.94° S) showed that the correlation is almost the same for all seasons, with a slight decrease in winter. Jicamarca has similar geomagnetic latitude to Ascension Island, which needs a detailed analysis of the seasonal variation in future work, due to the particularity of its location.
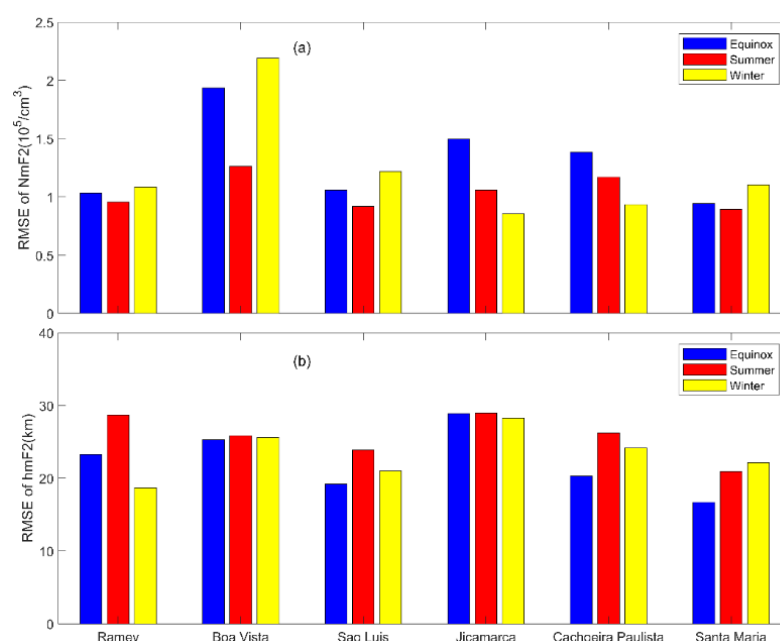

Figure 8. Seasonal RMSE of N_mF_2 (**a**) and h_mF_2 (**b**) during the equinox (blue), summer (red), and winter (yellow) periods at each station.

Figure 8b shows that, for the three seasonal RMSEs of h_mF_2, the RMSE values at all six ionosondes are under 30 km: the RMSEs at Ramey in summer are the highest, and the lowest during winter; while the RMSEs at Sao Luis, Cachoeira Paulista, and Santa Maria during the equinox season are the lowest; at Boa Vista and Jicamarca, there is no significant difference in the RMSE value of the three seasons. The seasonal mean $|Rel_E|$ results from the three periods of time are also analyzed in detail, which shows similar variations of RMSEs (see Table A3 in Appendix A for detailed seasonal RMSEs and seasonal mean $|Rel_E|$ of N_mF_2, and Table A4 in Appendix A for that of h_mF_2).

3.4. Variation Results during a Geomagnetic Storm

To investigate the COSMIC-2 variation results under geomagnetic storm conditions, data from 27–28 September 2020, during which time a moderate geomagnetic storm oc-

curred, were selected for study (detailed information on the storm can be found at: https://www.swpc.noaa.gov/news/g2-moderate-geomagnetic-storm-conditions-observed-4, accessed on 2 September 2021). Figure 9 shows the variation of the geomagnetic and solar activity parameter values during the period of 25–30 September 2020. Figure 9a indicates that the direction of the interplanetary magnetic field (IMF Bz) turns from northward to southward at 06:00UT on 27 September, implying that the motional electric field has the same direction as the dawn-to-dusk direction. This motional electric field likely leads to an upward dayside ionospheric plasma drift enhancement of the normal fountain effect [42]. Figure 9b shows that the flow pressure starts to increase from 0.67 nPa to 5.03 nPa at 14:00UT on 27 September; the solar wind speed shown in Figure 9d becomes stronger from 14:00UT on 27 September onward, with a solar wind speed of 480 km/s, and reaching the maximum of 684 km/s at 08:00UT on 28 September. Additionally, Figure 9c shows that the Dst index begins to decline at 19:00UT on 28 September, and reaches the minimum of −57 nT at 03:00UT on 28 September. Generally, a persistent southward IMF Bz and a dynamic pressure enhancement during enhanced solar wind speed cause increases in geomagnetic activity [43,44]. The variation of the geomagnetic and solar activity parameters in Figure 9 suggests a geomagnetic storm occurring late on 27 September, and lasting until 28 September.
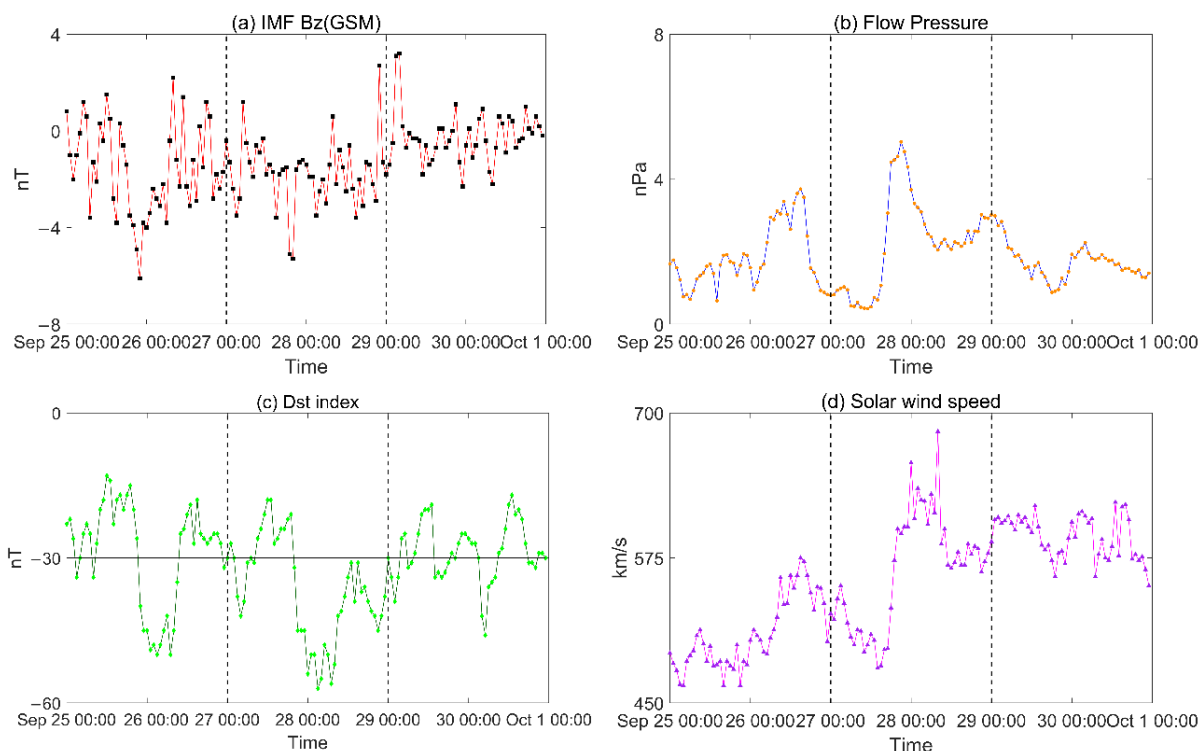
Figure 9. Variation in geomagnetic and solar parameter values during the period 25–30 September 2020, and the two vertical dashed lines denote the start and end moments of the period studied for a moderate geomagnetic storm condition.

As is shown in Figure 10, the variation of the absolute errors of $N_m F_2$ and $h_m F_2$ obtained from COSMIC-2 observations in comparison with the reference from ionosonde measurements during 27–28 September 2020, is presented (Table A5 in Appendix A shows geographic and geomagnetic locations of the ionosondes used). It should be noted that, for a given COSMIC-2 observation, its reference ionosonde station selected needs to be spatially co-located with the location of the COSMIC-2 observation, and the reference data selected from such a reference station also needs to be temporally simultaneous with the given COSMIC-2 observation. In this study, the co-location is defined as: a less than 3° latitudinal difference, and a less than 5° longitudinal difference. The simultaneity is defined as a less than a 1-h difference in observing times, which is because the 1-h difference in

observing time is the minimum time interval with a sufficient amount of data for analysis in this study. The absolute errors from these data pairs are shown in Figure 10, where the left column is for N_mF_2, and the right column is for h_mF_2. In each subfigure, the black line represents the geomagnetic equator; the edge of the shadow area is the terminator line; and the red and blue bars represent positive and negative values, respectively. We can see that most absolute errors for N_mF_2 are in the range of -0.3×10^6 to 0.3×10^6 el/cm^3, and the errors in the geomagnetic mid-latitude area are generally smaller than those of low latitudes. Furthermore, the left column of Figure 10 shows that at the same ionosonde station (except for stations Eglin Afb and Jicamarca), absolute value of the absolute error of N_mF_2 in Figure 10c is larger than that in all of the other three left-column subfigures. This implies that the absolute error of N_mF_2 rises during the geomagnetic storm period, but the amount of the variation is small. The right column shows that the absolute error values distribute in the range of -45 to 45 km, and the h_mF_2 derived from COSMIC-2 tends to be overestimated at most stations.
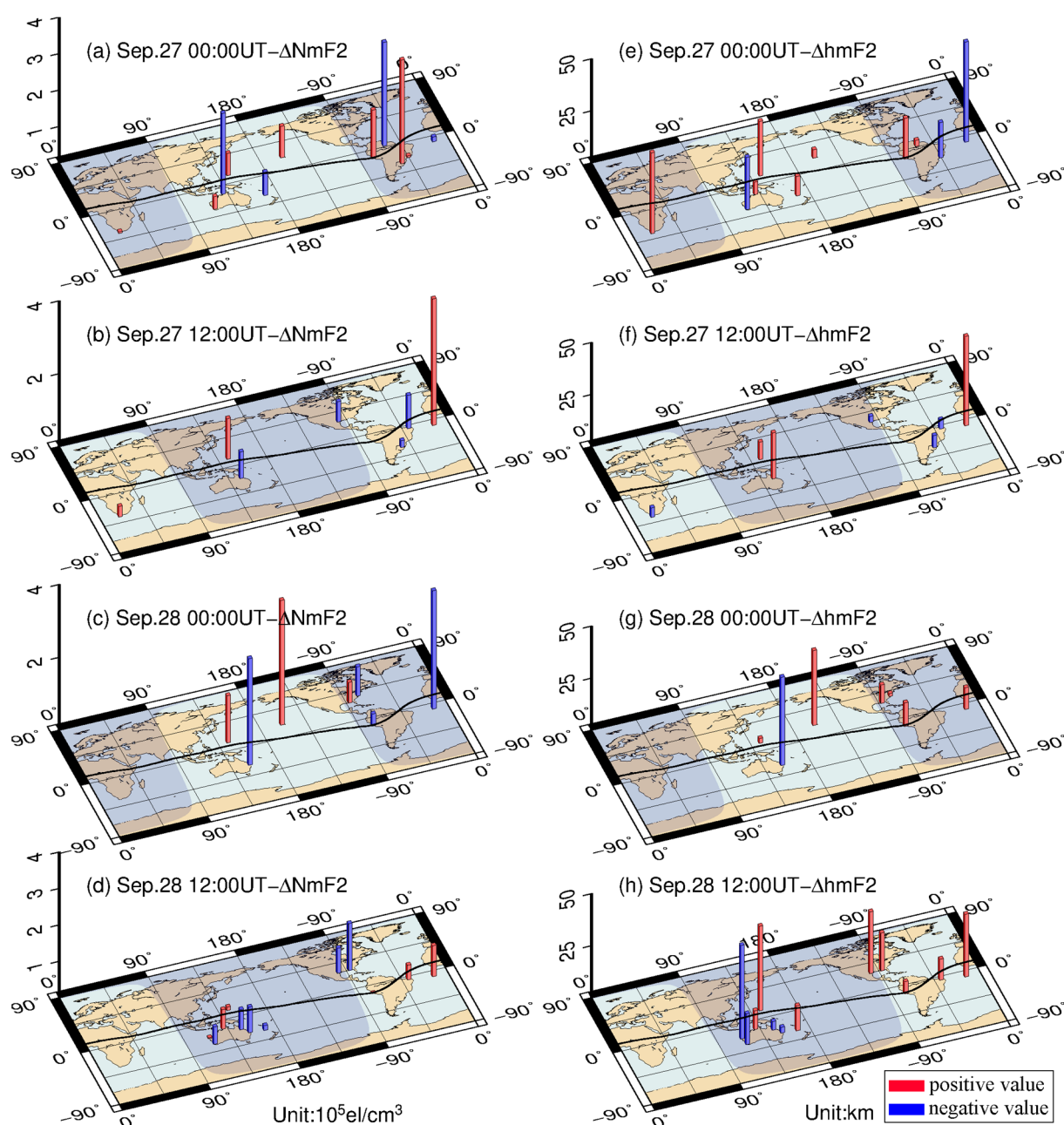

Figure 10. Snapshots for the absolute errors in N_mF_2 (**left column**) and h_mF_2 (**right column**) obtained from COSMIC-2

observations in comparison with the reference of ionosonde results during 27 September–28, 2020. In each subfigure, the black line represents the geomagnetic equator; the edge of the shadow area is the terminator line; the red and blue bars represent positive and negative values, respectively.

Wu et al. [45] used simulated ionospheric RO data to study the characteristics of the inversion error, and found that the relative inversion error was larger at low latitudes than at other latitudes; the main source of the inversion error was the spherical symmetry assumed for the distribution of electron density. Moreover, a comparison between the N_mF_2 measurements of COSMIC and ionosondes during a low solar activity year showed that the characteristics of the relative errors were consistent with that of the inversion errors. Furthermore, according to Yue et al. [18], electron density at low latitudes showed strong horizontal gradients, which did not comply with the assumption of spherical symmetry for electron density distribution. Thus, the errors in N_mF_2 in geomagnetic mid-latitude areas are smaller than at low latitudes. In addition, the enhancement of the equatorial fountain by the dawn-to-dusk electric field leads to the enhanced EIA crests at 00:00UT on 28 September, which is found in this study. In this case, the large inversion error caused by the large horizontal gradients may lead to larger absolute errors in N_mF_2 over the EIA region, as shown in Figure 10c.

It can also be seen from the left column that, at the Ascension Island station (7.95° S, 14.4° W, geomagnetic latitude 2.89° S), the absolute errors of N_mF_2 in the first and third panels, which are at 00:00UT on 27 and 28 September, tend to be underestimated (reflected by the blue bars); in the other two panels, which are at 12:00UT, they tend to be overestimated (reflected by the red bars). To understand this phenomenon, ionospheric electron densities on the meridian plane along the longitude of Ascension Island obtained from the IRI-2016 model are shown in Figure 11. The two right-column panels show that the Ascension Island station is expected to be located near the southern EIA crests. As a result, the slant TEC along the GPS signal is expected to experience a significant increase when transiting through it at 12:00UT. When the EDP is derived from COSMIC-2 RO, the increased slant TEC is expected to result in an overestimation of N_mF_2 over the Ascension Island station. The results of the observation follow a previous study, stating that the EIA crests contribute to the overestimation of N_mF_2 retrieved from COSMIC at the geomagnetic equator station of Jicamarca [15]. However, the two left-column panels indicate no apparent abnormal crest regions, and the variations of N_mF_2 obtained from COSMIC-2 at the Ascension Island station during nighttime need further research.

It also can be seen from Figure 10 that, compared with the absolute errors of N_mF_2 before the moderate geomagnetic storm, the absolute errors of N_mF_2 after the moderate geomagnetic storm do not significantly increase. Therefore, it is worth examining whether the electron density values obtained from COSMIC-2 have considerable variations during the period of the moderate geomagnetic storm. Due to the uneven distribution of the global ionosonde stations, and the absence of ionosonde stations on the sea, IRI-2016 was used to analyze the rationality of using COSMIC-2-derived electron densities for short-term dynamic evolution features analysis during the moderate geomagnetic storm. Figure 12 demonstrates the comparison in the distributions of electron density values obtained from COSMIC-2 RO profiles (top row) and IRI-2016 (bottom row) at 200, 300, and 400 km altitudes at 12:00UT on 27 September and 28 September. It can be seen that the distribution of electron density obtained from COSMIC-2 (the top two panels) cannot show the phenomena of EIA as clearly as the IRI-2016 model (the bottom two panels), which may be due to the amount of EDPs from COSMIC-2 at each moment being limited, and the EDPs being unevenly distributed. From the comparison between the bottom two panels (IRI results on two different days), hardly any differences can be found, meaning that the IRI-2016 model is unlikely to respond to the storm disturbance. This is consistent with the validation results of the IRI model—the IRI-2012, and also the IRI-2016 models do not correctly respond to storm disturbances [46–48]. However, the main difference between the top two panels is at the 300 km altitude (middle layer): the electron density in the right

panel is more enhanced over the Atlantic Ocean. This implies that COSMIC-2 results can capture the ionospheric dynamic feature under a moderate geomagnetic storm condition, unlike the IRI models, which perform poorly under geomagnetically disturbed conditions.
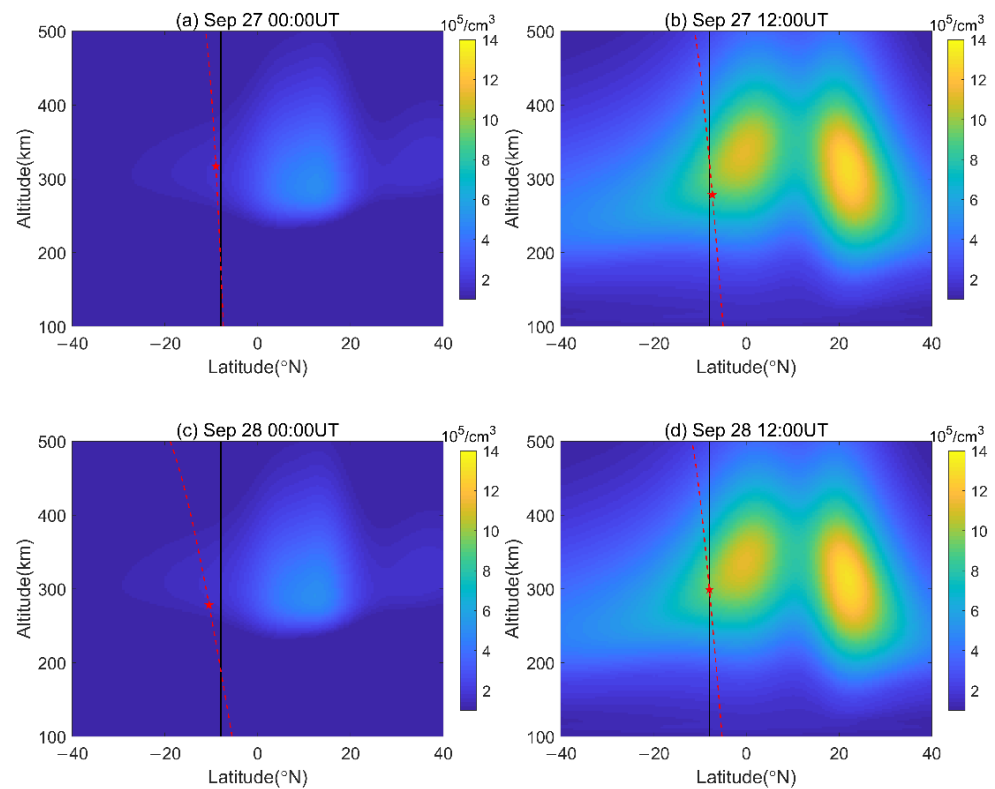
Figure 11. Snapshots of ionospheric electron density on the meridian plane along the longitude of the Ascension Island station obtained from the IRI-2016 model. The black vertical lines denote the Ascension Island latitude line; the red dashed lines are the lines between the tangent points of RO ray paths; and the pentagrams represent the location of the maximum electron density.
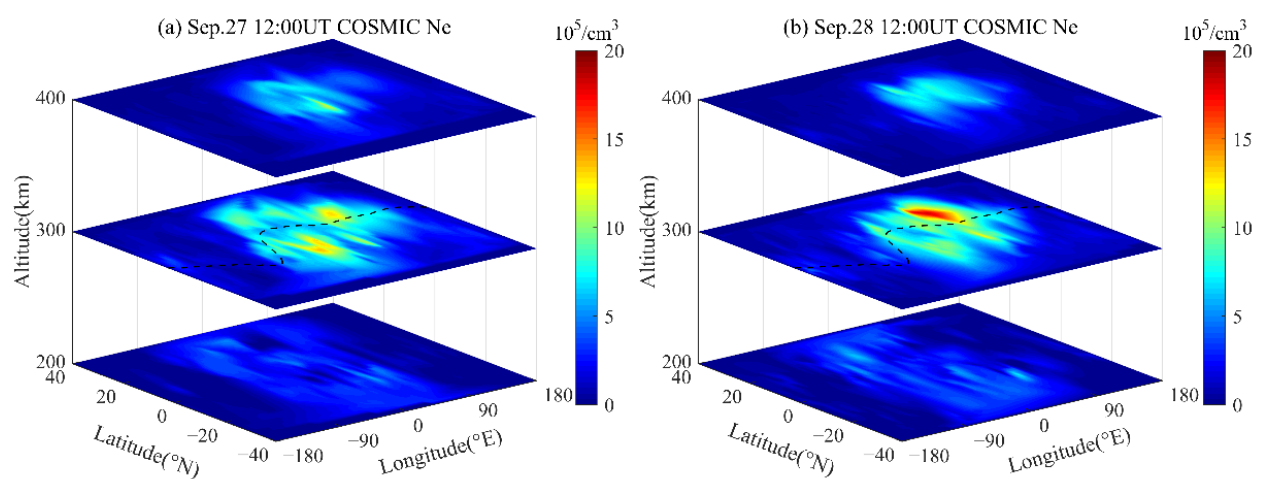
Figure 12. *Cont.*
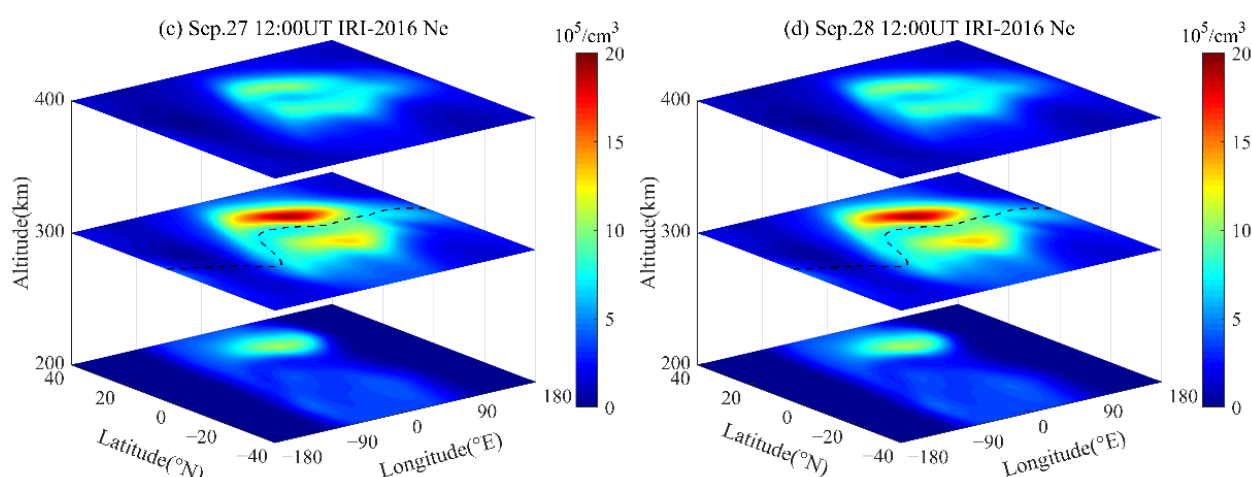
Figure 12. Snapshots of the distribution of electron density obtained from COSMIC-2 RO profiles (**top row**) and IRI-2016 model (**bottom row**) at 200, 300, and 400 km altitudes at 12:00UT on 27 September (**left column**) and 28 September (**right column**). The black dashed lines in slices of 300 km height are the magnetic equator lines.

4. Discussion

The test results presented in the above section suggest that COSMIC-2-derived ionospheric peak parameters agree well with the measurements of ionosondes. The error in the N_mF_2 obtained from COSMIC-2 and ionosonde measurement varies with latitude, especially in the EIA region, where the error is more notable. The spherical symmetry assumption for electron density distribution is found to be the main cause of the error in the retrieved COSMIC EDPs in the EIA region. Several studies have also found systematic overestimation/underestimation of the N_mF_2 retrieved from COSMIC RO in the EIA region, due to the violation of the spherical symmetry assumed for the Abel inversion in this region [15,17,19,36]. Tsai et al. [19] examined electron density profiles from GPS/MET and ionosonde measurements at Chung-Li (24.6° N, 121.0° E; 14° N geomagnetic) during a 67-day period, and results showed that the GPS/MET derived N_mF_2 was underestimated during the afternoon and early evening periods. This implied an asymmetric structure in the north EIA region, and the fountain effect of the vertical electrodynamics drifts at the equator, and plasma diffusion along geomagnetic field lines most likely caused this phenomenon. Liu et al. [15] stated an overestimation of COSMIC-derived N_mF_2 at Jicamarca, a geomagnetic equator station, during the afternoon period. This was most likely due to the invalid assumption of spherical symmetry in the pronounced EIA regions. The test results from this research also show the similar variation tendency when the EIA is well developed during daytime, and, in this case, more intense latitudinal gradients in electron density present, and an overestimation/underestimation of COSMIC-2 derived N_mF_2 generally occurs at Jicamarca/Boa Vista. In addition, Chu et al. [40] compared two h_mF_2 datasets obtained from COSMIC and ionosonde (using the Titheridge method), and found that the former is generally larger than the latter. In this study, h_mF_2 is obtained from manually scaled ionograms using the SAO Explorer software. Although this method is different from the Titheridge method, its results are similar to that of Titheridge method. The results in the right column of Figures 6 and 7 indicate that the true peak height tends to be underestimated by h_mF_2 derived from ionosondes, based on the ARTIST method. Furthermore, this study demonstrates that the Abel inversion method under the spherical symmetry assumption of electron density distribution introduces larger errors to COSMIC-2 EDPs at low latitudes, where the electron density has large horizontal gradients. It is believed that data quality validation of COSMIC-2-derived ionospheric peak parameters will be an important step in further ionospheric research on the use of COSMIC-2 data in low-latitude regions.

5. Conclusions and Perspectives

In this study, IPPVs obtained from COSMIC-2 RO data were validated by comparing them against the reference of the measurements of six ionosondes over low-latitude regions of the Americas during the approximately 2-year period from 1 October 2019, to 31 August 2021. The performances of the IPPVs in different latitudinal regions, in different hours of day and different seasons, as well as in the duration of a moderate geomagnetic storm, were analyzed. The results illustrated that the COSMIC-2-derived IPPVs agreed well with the ones from ionosondes, with the correlation coefficients for the two sets of data for N_mF_2 (h_mF_2) at Ramey, Boa Vista, Sao Luis, Jicamarca, Cachoeira Paulista, and Santa Maria being 0.93 (0.84), 0.91 (0.85), 0.91 (0.88), 0.88 (0.79), 0.96 (0.83), and 0.96 (0.87), respectively, whereas the neglect of the large horizontal gradients in the retrieval of electron density profiles introduce significant errors in low geomagnetic latitude regions (e.g., at Boa Vista). In general, the N_mF_2 values derived from COSMIC-2 at the Sao Luis and Jicamarca stations, which are close to the geomagnetic equator, tend to be overestimated, whilst the results at the Boa Vista and Cachoeira Paulista stations, which are close to the EIA crests, are underestimated. This is because, when the COSMIC-2 RO EDPs are retrieved by the Abel inversion under the assumption of spherical symmetry, the horizontal gradient of the TEC along the GPS ray is affected by the EIA, which may introduce errors to the EDPs. The larger electron density along the GPS ray path will be averaged, which enlarges the original small electron density values. Furthermore, h_mF_2 obtained from COSMIC-2 tends to be overestimated at all the six stations tested.

The absolute errors of N_mF_2 varied with geomagnetic latitude with the RMSE of N_mF_2 at Ramey, Boa Vista, Sao Luis, Jicamarca, Cachoeira Paulista, and Santa Maria are 1.00×10^5 el/cm³, 1.76×10^5 el/cm³, 1.10×10^5 el/cm³, 1.26×10^5 el/cm³, 1.35×10^5 el/cm³, and 0.99×10^5 el/cm³, respectively. Moreover, the relative errors for N_mF_2 and h_mF_2 indicated that the COSMIC-2-derived h_mF_2 obtained by the Abel inversion algorithm was better than N_mF_2. N_mF_2 and h_mF_2 obtained from COSMIC-2 and ionosonde measurements showed the same trend of diurnal variation, and had a good agreement at all six stations. When the EIA was well developed during daytime, COSMIC-2 derived N_mF_2 was, on average, overestimated/underestimated at the stations of Jicamarca/Boa Vista. Seasonal results showed that at Ramey, Boa Vista, Sao Luis, and Santa Maria stations, the minimum and maximum of the RMSEs of N_mF_2 occurred during summer and winter, respectively; at Jicamarca and Cachoeira Paulista, the minimum and maximum occur in winter (yellow) and equinox (blue), respectively. The absolute error of N_mF_2 rose during a geomagnetic storm period, but the fluctuation value was small. Furthermore, electron density obtained from COSMIC-2 was better in the capturing of the ionospheric dynamic enhancements under moderate geomagnetic storm conditions, unlike the IRI-2016 model, which performed poorly under geomagnetically disturbed conditions.

This study gives detailed validation of COSMIC-2-derived IPPVs over low-latitude regions of the Americas. Since the low solar activity period selected for comparing COSMIC-2-IPPVs and ionosonde-IPPVs conducted in this study is relatively short, our future work will focus on using long-term data to further assess the COSMIC-2-IPPVs. Furthermore, long-term data also should be used to validate the data quality of COSMIC-2-IPPVs during periods of high solar activity and geomagnetic disturbances.

Author Contributions: Conceptualization, S.S. and K.Z.; methodology, S.S. and W.L.; software, F.S. and J.S.; validation, S.S., W.L. and P.S.; formal analysis, S.S. and W.L.; writing—original draft preparation, S.S. and W.L.; writing—review and editing, S.S., S.W. and K.Z.; funding acquisition, K.Z. All authors have read and agreed to the published version of the manuscript.

Appendix A

Table A1. Statistics of the differences in N_mF_2 obtained from the COSMIC-2 and ionosonde (as the reference) at the six ionosondes under quiet geomagnetic conditions in terms of hourly RMSE (10^5 el/cm^3) and hourly mean $|Rel_E|$ (MRE, %).

LT	Ramey		Boa Vista		Sao Luis		Jicamarca		Cachoeira Paulista		Santa Maria	
	RMSE	MRE	RMSE	MRE	RMSE	MRE	RMSE	MRE	RMSE	MRE	RMSE	MRE
1	0.90	20.50	1.39	29.56	0.66	29.50	1.07	23.11	0.60	61.02	0.28	18.73
2	0.74	19.85	1.37	22.24	0.35	20.41	0.93	28.04	0.26	23.21	0.16	10.08
3	0.52	18.57	0.43	19.69	0.52	55.22	0.64	24.11	0.65	47.82	0.39	17.80
4	0.51	21.30	0.37	19.05	0.22	13.93	0.73	35.94	0.21	15.01	0.11	16.18
5	0.48	20.91	0.23	22.28	0.34	30.81			0.25	16.04	0.44	21.29
6	0.61	26.88	0.48	26.68	1.25	37.99	0.92	29.80	0.42	29.01	0.39	18.81
7	0.47	14.93	1.06	22.28			0.71	14.34			0.38	9.91
8	0.41	9.84	1.74	39.87	0.92	12.10	0.67	10.76	0.47	10.67	0.41	10.05
9	0.57	12.37	1.57	30.72	1.22	14.63	1.04	12.13	0.52	9.67	0.49	11.11
10	0.76	13.41	1.78	18.35	0.94	11.37	1.00	13.48	0.67	10.65	0.67	10.82
11	0.80	14.77	2.33	20.53	1.25	13.40	1.09	13.92	0.87	11.57	1.07	14.74
12	0.91	13.95	2.19	19.03	1.18	13.01	0.79	9.30	1.02	11.80	1.21	14.48
13	1.08	13.95	1.70	14.01	1.19	14.02	1.20	12.90	1.19	14.97	0.82	9.46
14	1.81	18.13	2.02	14.06	1.00	11.35	1.36	15.83	1.25	12.89	1.00	13.20
15	1.62	16.54	1.97	14.92	1.04	11.13	2.00	24.22	1.26	12.81	1.20	16.75
16	1.44	13.17	2.01	14.25	1.09	10.47	1.14	13.32	1.65	15.11	1.42	20.16
17	1.46	14.38	2.31	16.22	1.19	12.25	1.20	13.92	1.51	16.26	2.37	38.69
18	1.39	13.95	1.70	14.81	1.24	16.74	1.46	16.52	2.24	25.64	1.54	31.83
19	2.02	27.07	2.14	18.02	1.04	18.51	1.35	20.73	1.44	24.28	0.80	16.08
20	1.50	27.56	1.63	23.65	1.08	19.81	1.45	24.46	1.73	50.46	0.40	10.81
21	0.88	20.74	0.98	20.55	1.64	25.81	2.20	31.24	1.54	49.40	0.45	14.26
22	0.66	15.59	0.60	19.01	1.71	26.32	0.97	20.79	0.97	49.22	1.37	38.92
23	1.12	21.05	0.63	23.67	0.73	22.99	1.56	24.33	1.06	48.97	0.36	16.72
24	0.75	17.20	0.99	19.94	0.21	9.73	0.96	19.46	0.29	21.59	0.33	15.69

Table A2. Statistics of the differences in h_mF_2 obtained from the COSMIC-2 and ionosonde (as the reference) at the six ionosondes under quiet geomagnetic conditions in terms of hourly RMSE (km) and hourly mean |RelE| (MRE, %).

LT	Ramey		Boa Vista		Sao Luis		Jicamarca		Cachoeira Paulista		Santa Maria	
	RMSE	MRE	RMSE	MRE	RMSE	MRE	RMSE	MRE	RMSE	MRE	RMSE	MRE
1	27.39	6.41	33.00	7.47	38.40	15.72	32.81	9.46	42.38	11.08	29.34	6.09
2	24.06	6.30	17.11	4.79	37.83	11.52	27.32	7.89	34.32	9.82	40.92	6.99
3	27.11	7.10	21.20	5.25	29.84	9.28	34.05	9.10	34.30	9.86	18.03	5.38
4	23.24	6.46	19.84	4.93	13.62	4.05	37.68	13.10	25.96	6.12	22.14	6.54
5	25.02	6.57	28.13	8.39	32.57	9.46			24.38	5.87	19.74	6.06
6	26.57	7.80	33.55	9.18	14.55	4.31	16.08	5.91	27.00	8.21	13.59	4.26
7	16.73	6.09	17.36	5.35			19.79	6.27			14.21	5.19
8	13.76	5.32	35.29	11.78	17.13	4.68	21.94	6.18	32.00	7.57	19.94	7.34
9	20.21	7.13	37.89	11.12	22.54	5.79	26.38	7.13	17.24	5.00	20.56	7.04
10	19.81	6.85	24.10	6.61	22.05	5.30	27.18	7.83	19.17	5.35	18.59	5.85
11	33.07	11.09	28.38	7.50	26.76	6.15	29.75	8.01	15.68	4.73	22.43	7.60
12	32.38	10.08	26.36	6.70	25.96	6.01	33.25	8.22	15.37	4.77	18.12	5.62
13	30.09	9.44	26.71	6.15	26.01	5.49	23.41	6.44	21.26	7.00	18.01	6.36
14	27.08	8.32	26.36	6.00	21.00	4.94	26.75	6.81	19.33	5.55	16.97	5.49
15	22.65	6.27	26.67	6.82	16.47	4.02	36.58	9.95	15.09	4.30	15.05	4.55
16	14.36	4.27	22.26	5.31	17.67	4.66	27.05	6.29	13.76	4.52	16.23	5.80
17	28.10	7.92	23.96	5.60	15.10	4.10	29.49	6.61	15.64	4.92	13.60	4.61
18	15.79	5.19	19.78	4.87	17.68	4.31	29.65	7.71	15.82	4.76	25.42	8.10
19	26.63	6.71	17.40	4.17	20.41	4.79	37.93	8.90	29.57	6.47	24.03	7.28
20	33.05	8.43	18.53	4.70	24.63	6.96	29.33	7.45	50.48	11.83	29.43	8.00
21	34.17	8.94	20.59	4.27	35.98	10.57	36.98	9.51	36.71	9.54	28.20	7.05
22	28.44	7.07	20.77	4.42	31.25	9.39	32.47	8.95	43.37	10.29	35.19	10.09
23	20.61	4.82	22.53	4.49	30.23	9.46	38.02	10.84	33.84	8.14	12.92	4.12
24	22.87	4.85	20.28	4.78	39.44	11.66	31.03	9.42	33.68	8.86	10.39	2.82

Table A3. Statistics of the differences in N_mF_2 obtained from the COSMIC-2 and ionosonde (as the reference) at the six ionosondes under quiet geomagnetic conditions in terms of RMSE (10^5 el/cm^3) and mean |RelE| (MRE, %) in different seasons.

Season	Ramey		Boa Vista		Sao Luis		Jicamarca		Cachoeira Paulista		Santa Maria	
	RMSE	MRE	RMSE	MRE	RMSE	MRE	RMSE	MRE	RMSE	MRE	RMSE	MRE
equinox	1.03	19.99	1.94	21.74	1.06	13.80	1.50	35.18	1.38	13.99	0.94	14.20
summer	0.96	18.64	1.26	18.20	0.92	11.71	1.06	28.07	1.17	11.17	0.89	9.52
winter	1.09	22.93	2.19	24.01	1.22	22.74	0.85	22.44	0.93	10.23	1.10	18.98

Table A4. Statistics of the differences in h_mF_2 obtained from the COSMIC-2 and ionosonde (as the reference) at the six ionosondes under quiet geomagnetic conditions in terms of RMSE (km) and mean |RelE| (MRE, %) in different seasons.

Season	Ramey		Boa Vista		Sao Luis		Jicamarca		Cachoeira Paulista		Santa Maria	
	RMSE	MRE	RMSE	MRE	RMSE	MRE	RMSE	MRE	RMSE	MRE	RMSE	MRE
equinox	23.30	6.11	25.29	5.87	19.22	4.69	28.90	7.83	20.30	5.06	16.71	5.15
summer	28.70	7.22	25.86	5.94	23.87	5.54	28.95	7.47	26.22	6.77	20.95	5.99
winter	18.69	5.57	25.60	5.74	21.01	5.43	28.28	7.22	24.15	6.21	22.17	6.38

Table A5. Geographic and geomagnetic locations of the ionosondes used during 27–28 September 2020 ('x' indicates that the ionosonde was used at the specific time).

Station	Geog. Lon. (° E)	Geog. Lat. (° N)	Geom. Lat. (° N)	Sep. 27 00:00UT	Sep. 27 12:00UT	Sep. 28 00:00UT	Sep. 28 12:00UT
Ascension Island	−14.40	−7.95	−2.89	x	x	x	x
Boa Vista	−60.70	2.80	11.98	x			
Cachoeira Paulista	−45.00	−22.70	−14.17	x			
Darwin	130.95	−12.45	−20.96	x			x
Guam	144.86	13.62	6.02	x	x	x	x
Hermanus	19.22	−34.42	−34.03	x	x		
Jicamarca	−76.80	−12.00	−2.54	x		x	x
Lualualei	−158.15	21.43	21.74	x		x	
Norfolk	167.97	−29.03	−33.13	x			x
Perth	116.13	−32.00	−41.11	x			x
Santa Maria	−53.71	−29.73	−20.63	x	x		
Austin	−97.70	30.40	38.66		x		x
Fortaleza	−38.40	−3.90	3.91		x		x
Townsville	146.85	−19.63	−26.64		x		x
Brisbane	153.06	−27.06	−33.24			x	x
Eglin Afb	−86.50	30.50	39.44			x	x
Wallops Is	−75.50	37.90	47.11			x	
Learmonth	114.10	−21.80	−31.01				x

References

1. Kursinski, E.R.; Hajj, G.A.; Schofield, J.T.; Linfield, R.P.; Hardy, K.R. Observing Earth's atmosphere with radio occultation measurements using the Global Positioning System. *J. Geophys. Res. Atmos.* **1997**, *102*, 23429–23465. [CrossRef]
2. Hu, A.; Wu, S.; Wang, X.; Wang, Y.; Norman, R.; He, C.; Cai, H.; Zhang, K. Improvement of reflection detection success rate of GNSS RO measurements using artificial neural network. *IEEE Trans. Geosci. Remote Sens.* **2018**, *56*, 760–769. [CrossRef]
3. Banos, I.H.; Sapucci, L.F.; Cucurull, L.; Bastarz, C.F.; Silveira, B.B. Assimilation of GPSRO bending angle profiles into the Brazilian global atmospheric model. *Remote Sens.* **2019**, *11*, 256. [CrossRef]
4. Sokolovskiy, S.V.; Rocken, C.; Lenschow, D.H.; Kuo, Y.H.; Anthes, R.A.; Schreiner, W.S.; Hunt, D.C. Observing the moist troposphere with radio occultation signals from COSMIC. *Geophys. Res. Lett.* **2007**, *34*, 1–6. [CrossRef]
5. Foelsche, U.; Pirscher, B.; Borsche, M.; Kirchengast, G.; Wickert, J. Assessing the climate monitoring utility of radio occultation data: From CHAMP to FORMOSAT-3/COSMIC. *Terr. Atmos. Ocean. Sci.* **2009**, *20*, 155–170. [CrossRef]
6. Tsuda, T.; Lin, X.; Hayashi, H. Analysis of vertical wave number spectrum of atmospheric gravity waves in the stratosphere using COSMIC GPS radio occultation data. *Atmos. Meas. Tech.* **2011**, *4*, 1627–1636. [CrossRef]
7. Johnston, B.; Xie, F. Characterizing extratropical tropopause bimodality and its relationship to the occurrence of double tropopauses using COSMIC GPS radio occultation observations. *Remote Sens.* **2020**, *12*, 1109. [CrossRef]
8. Lin, C.H.; Liu, J.Y.; Fang, T.W.; Chang, P.Y.; Tsai, H.F.; Chen, C.H.; Hsiao, C.C. Motions of the equatorial ionization anomaly crests imaged by FORMOSAT-3/COSMIC. *Geophys. Res. Lett.* **2007**, *34*, L19101. [CrossRef]
9. Lin, C.H.; Wang, W.; Hagan, M.E.; Hsiao, C.C.; Immel, T.J.; Hsu, M.L.; Liu, J.Y.; Paxton, L.J.; Fang, T.W.; Liu, C.H. Plausible effect of atmospheric tides on the equatorial ionosphere observed by the FORMOSAT-3/COSMIC: Three-dimensional electron density structures. *Geophys. Res. Lett.* **2007**, *34*, 1–5. [CrossRef]
10. He, M.; Liu, L.; Wan, W.; Ning, B.; Zhao, B.; Wen, J.; Yue, X.a.; Le, H. A study of the Weddell Sea Anomaly observed by FORMOSAT-3/COSMIC. *J. Geophys. Res. Space Phys.* **2009**, *114*, 1–10. [CrossRef]
11. Liu, J.Y.; Lin, C.Y.; Lin, C.H.; Tsai, H.F.; Solomon, S.C.; Sun, Y.Y.; Lee, I.T.; Schreiner, W.S.; Kuo, Y.H. Artificial plasma cave in the low-latitude ionosphere results from the radio occultation inversion of the FORMOSAT-3/COSMIC. *J. Geophys. Res. Space Phys.* **2010**, *115*, 1–8. [CrossRef]
12. Zakharenkova, I.E.; Krankowski, A.; Shagimuratov, I.I.; Cherniak, Y.V.; Krypiak-Gregorczyk, A.; Wielgosz, P.; Lagovsky, A.F. Observation of the ionospheric storm of October 11, 2008 using FORMOSAT-3/COSMIC data. *EarthPlanets Space* **2012**, *64*, 505–512. [CrossRef]
13. Lin, C.-H.; Liu, J.-Y.; Hsiao, C.-C.; Liu, C.-H.; Cheng, C.-Z.; Chang, P.-Y.; Tsai, H.-F.; Fang, T.-W.; Chen, C.-H.; Hsu, M.-L. Global ionospheric structure imaged by FORMOSAT-3/COSMIC: Early results. *Terr. Atmos. Ocean. Sci.* **2009**, *20*, 171–179. [CrossRef]
14. Zhao, B.; Wan, W.; Yue, X.; Liu, L.; Ren, Z.; He, M.; Liu, J. Global characteristics of occurrence of an additional layer in the ionosphere observed by COSMIC/FORMOSAT-3. *Geophys. Res. Lett.* **2011**, *38*, 1–5. [CrossRef]
15. Liu, J.-Y.; Lee, C.-C.; Yang, J.-Y.; Chen, C.-Y.; Reinisch, B.W. Electron density profiles in the equatorial ionosphere observed by the FORMOSAT-3/COSMIC and a digisonde at Jicamarca. *GPS Solut.* **2010**, *14*, 75–81. [CrossRef]

16. Krankowski, A.; Zakharenkova, I.; Krypiak-Gregorczyk, A.; Shagimuratov, I.I.; Wielgosz, P. Ionospheric electron density observed by FORMOSAT-3/COSMIC over the European region and validated by ionosonde data. *J. Geod.* **2011**, *85*, 949–964. [CrossRef]

17. Hajj, G.A.; Romans, L.J. Ionospheric electron density profiles obtained with the Global Positioning System: Results from the GPS/MET experiment. *Radio Sci.* **1998**, *33*, 175–190. [CrossRef]

18. Yue, X.; Schreiner, W.S.; Lei, J.; Sokolovskiy, S.V.; Rocken, C.; Hunt, D.C.; Kuo, Y.H. Error analysis of Abel retrieved electron density profiles from radio occultation measurements. *Ann. Geophys.* **2010**, *28*, 217–222. [CrossRef]

19. Tsai, L.C.; Tsai, W.H.; Schreiner, W.S.; Berkey, F.T.; Liu, J.Y. Comparisons of GPS/MET retrieved ionospheric electron density and ground based ionosonde data. *EarthPlanets Space* **2001**, *53*, 193–205. [CrossRef]

20. Lei, J.; Syndergaard, S.; Burns, A.G.; Solomon, S.C.; Wang, W.; Zeng, Z.; Roble, R.G.; Wu, Q.; Kuo, Y.-H.; Holt, J.M.; et al. Comparison of COSMIC ionospheric measurements with ground-based observations and model predictions: Preliminary results. *J. Geophys. Res. Space Phys.* **2007**, *112*, 1–10. [CrossRef]

21. Yang, K.-F.; Chu, Y.-H.; Su, C.-L.; Ko, H.-T.; Wang, C.-Y. An examination of FORMOSAT-3/COSMIC ionospheric electron density profile: Data quality criteria and comparisons with the IRI model. *Terr. Atmos. Ocean. Sci.* **2009**, *20*, 193–206. [CrossRef]

22. Ely, C.V.; Batista, I.S.; Abdu, M.A. Radio occultation electron density profiles from the FORMOSAT-3/COSMIC satellites over the Brazilian region: A comparison with Digisonde data. *Adv. Space Res.* **2012**, *49*, 1553–1562. [CrossRef]

23. Cherniak, I.V.; Zakharenkova, I.E. Validation of FORMOSAT-3/COSMIC radio occultation electron density profiles by incoherent scatter radar data. *Adv. Space Res.* **2014**, *53*, 1304–1312. [CrossRef]

24. Hu, L.; Ning, B.; Liu, L.; Zhao, B.; Chen, Y.; Li, G. Comparison between ionospheric peak parameters retrieved from COSMIC measurement and ionosonde observation over Sanya. *Adv. Space Res.* **2014**, *54*, 929–938. [CrossRef]

25. Hu, L.; Ning, B.; Liu, L.; Zhao, B.; Li, G.; Wu, B.; Huang, Z.; Hao, X.; Chang, S.; Wu, Z. Validation of COSMIC ionospheric peak parameters by the measurements of an ionosonde chain in China. *Ann. Geophys.* **2014**, *32*, 1311–1319. [CrossRef]

26. McNamara, L.F.; Thompson, D.C. Validation of COSMIC values of foF2 and M(3000)F2 using ground-based ionosondes. *Adv. Space Res.* **2015**, *55*, 163–169. [CrossRef]

27. Luo, J.; Sun, F.; Xu, X.; Wang, H. Ionospheric F2-Layer critical frequency retrieved from COSMIC radio occultation: A statistical comparison with measurements from a meridional ionosonde chain over Southeast Asia. *Adv. Space Res.* **2019**, *63*, 327–336. [CrossRef]

28. Bilitza, D.; Altadill, D.; Truhlik, V.; Shubin, V.; Galkin, I.; Reinisch, B.; Huang, X. International Reference Ionosphere 2016: From ionospheric climate to real-time weather predictions. *Space Weather* **2017**, *15*, 418–429. [CrossRef]

29. Bilitza, D. IRI the International Standard for the Ionosphere. *Adv. Radio Sci.* **2018**, *16*, 1–11. [CrossRef]

30. Lin, C.Y.; Lin, C.C.H.; Liu, J.Y.; Rajesh, P.K.; Matsuo, T.; Chou, M.Y.; Tsai, H.F.; Yeh, W.H. The early results and validation of FORMOSAT-7/COSMIC-2 space weather products: Global ionospheric specification and Ne-Aided Abel electron density profile. *J. Geophys. Res. Space Phys.* **2020**, *125*, e2020JA028028. [CrossRef]

31. Cherniak, I.; Zakharenkova, I.; Braun, J.; Wu, Q.; Pedatella, N.; Schreiner, W.; Weiss, J.-P.; Hunt, D. Accuracy assessment of the quiet-time ionospheric F2 peak parameters as derived from COSMIC-2 multi-GNSS radio occultation measurements. *J. Space Weather Space Clim.* **2021**, *11*, 18. [CrossRef]

32. Okoh, D.; Seemala, G.; Rabiu, B.; Habarulema, J.B.; Jin, S.; Shiokawa, K.; Otsuka, Y.; Aggarwal, M.; Uwamahoro, J.; Mungufeni, P.; et al. A neural network-based ionospheric model over Africa from Constellation Observing System for Meteorology, Ionosphere, and Climate and ground Global Positioning System observations. *J. Geophys. Res. Space Phys.* **2019**, *124*, 10512–10532. [CrossRef]

33. Li, W.; Zhao, D.; He, C.; Hu, A.; Zhang, K. Advanced machine learning optimized by the genetic algorithm in ionospheric models using long-term multi-instrument observations. *Remote Sens.* **2020**, *12*, 866. [CrossRef]

34. Cander, L.R.; Mihajlovic, S.J. Forecasting ionospheric structure during the great geomagnetic storms. *J. Geophys. Res. Space Phys.* **1998**, *103*, 391–398. [CrossRef]

35. Kumar, S.; Singh, R.P.; Tan, E.L.; Singh, A.K.; Ghodpage, R.N.; Siingh, D. Temporal and spatial deviation in F2 peak parameters derived from FORMOSAT-3/COSMIC. *Space Weather* **2016**, *14*, 391–405. [CrossRef]

36. Schreiner, W.S.; Sokolovskiy, S.V.; Rocken, C.; Hunt, D.C. Analysis and validation of GPS/MET radio occultation data in the ionosphere. *Radio Sci.* **1999**, *34*, 949–966. [CrossRef]

37. Reinisch, B.W.; Huang, X. Automatic calculation of electron density profiles from digital ionograms: 3. Processing of bottomside ionograms. *Radio Sci.* **1983**, *18*, 477–492. [CrossRef]

38. Galkin, I.A.; Khmyrov, G.M.; Kozlov, A.V.; Reinisch, B.W.; Huang, X.; Paznukhov, V.V. The ARTIST 5. *AIP Conf. Proc.* **2008**, *974*, 150–159. [CrossRef]

39. Reinisch, B.W.; Galkin, I.A. Global Ionospheric Radio Observatory (GIRO). *EarthPlanets Space* **2011**, *63*, 377–381. [CrossRef]

40. Chu, Y.-H.; Su, C.-L.; Ko, H.-T. A global survey of COSMIC ionospheric peak electron density and its height: A comparison with ground-based ionosonde measurements. *Adv. Space Res.* **2010**, *46*, 431–439. [CrossRef]

41. Chuo, Y.J.; Lee, C.C.; Chen, W.S.; Reinisch, B.W. Comparison of the characteristics of ionospheric parameters obtained from FORMOSAT-3 and digisonde over Ascension Island. *Ann. Geophys.* **2013**, *31*, 787–794. [CrossRef]

42. Tsurutani, B.T.; Verkhoglyadova, O.P.; Mannucci, A.J.; Saito, A.; Araki, T.; Yumoto, K.; Tsuda, T.; Abdu, M.A.; Sobral, J.H.A.; Gonzalez, W.D.; et al. Prompt penetration electric fields (PPEFs) and their ionospheric effects during the great magnetic storm of 30–31 October 2003. *J. Geophys. Res. Space Phys.* **2008**, *113*, 1–10. [CrossRef]

43. Boudouridis, A.; Zesta, E.; Lyons, L.R.; Anderson, P.C.; Lummerzheim, D. Enhanced solar wind geoeffectiveness after a sudden increase in dynamic pressure during southward IMF orientation. *J. Geophys. Res.* **2005**, *110*, 1–15. [CrossRef]

44. Adebesin, B.O.; Ikubanni, S.O.; Kayode, J.S. Solar wind dynamic pressure depency on the plasma flow speed and IMF Bz during different geomagnetic activities. *World J. Young Res.* **2012**, *2*, 43–54.

45. Wu, X.; Hu, X.; Gong, X.; Zhang, X.; Wang, X. Analysis of inversion errors of ionospheric radio occultation. *GPS Solut.* **2009**, *13*, 231–239. [CrossRef]

46. Kumar, S.; Tan, E.L.; Razul, S.G.; See, C.M.S.; Siingh, D. Validation of the IRI-2012 model with GPS-based ground observation over a low-latitude Singapore station. *EarthPlanets Space* **2014**, *66*, 1–17. [CrossRef]

47. Timoçin, E.; Ünal, İ.; Göker, Ü.D. A comparison of IRI-2016 foF2 predictions with the observations at different latitudes during geomagnetic storms. *Geomagn. Aeron.* **2019**, *58*, 846–856. [CrossRef]

48. Endeshaw, L. Testing and validating IRI-2016 model over Ethiopian ionosphere. *Astrophys. Space Sci.* **2020**, *365*, 1–13. [CrossRef]